

Molecular Modeling and Simulation of Vapor-Liquid Equilibria of Ethylene oxide, Ethylene glycol and Water as well as their Binary Mixtures

Y.-L. Huang,[†] T. Merker,[‡] M. Heilig,[¶] H. Hasse,[‡] and J. Vrabec^{*,†}

*Thermodynamics and Energy Technology, University of Paderborn, 33098 Paderborn, Germany,
Laboratory of Engineering Thermodynamics, University of Kaiserslautern, 67633 Kaiserslautern,
Germany, and GCP Chemical and Process Engineering, BASF SE, Ludwigshafen, Germany*

E-mail: jadran.vrabec@upb.de

Abstract

Mixtures containing ethylene oxide are technically highly relevant but hazardous so that typically only few reliable experimental data are available. They are therefore interesting candidates for the application of molecular modeling and simulation to predict thermodynamic properties. The industrially most important ethylene oxide containing mixtures are those with water and ethylene glycol. An excellent molecular model for ethylene oxide is available from prior work. Because the molecular models for water from the literature do not yield satisfactory results for the vapor-liquid equilibrium over a wide temperature range, a new water model is developed. Furthermore, also a new molecular model for ethylene glycol is developed. The models for Ethylene glycol and Water show mean unsigned deviations with respect to experimental data, considering the whole temperature range from triple point to critical point, of

*To whom correspondence should be addressed

[†]University of Paderborn

[‡]University of Kaiserslautern

[¶]BASF SE

0.8 % and 1.1 % for the saturated liquid density, 4.8 % and 7.2 % for the vapor pressure, and 13.4 % and 2.8 % for the enthalpy of vaporization, respectively. Vapor-liquid equilibria of all three binary mixtures are determined by molecular simulation and in general, a good agreement is found with the available experimental data. The models can be used for subsequent predictions at other conditions.

Keywords: Force field; Molecular modeling; vapor-liquid equilibrium; critical properties; Ethylene oxide, Ethylene glycol, Water

Introduction

Molecular modeling and simulation are based on mathematical representations of the intermolecular interactions so that it has strong predictive capabilities, as it adequately covers structure, energetics and dynamics on the microscopic scale that govern the fluid behavior on the macroscopic scale.

Backed by the chemical industry, substantial efforts were made in recent years by the molecular simulation community to tackle the thermophysical properties of technically relevant fluid systems.¹⁻⁵ This is particularly rewarding for substances with hazardous properties that render experimental studies difficult. The present work was carried out in an academic-industrial cooperation and follows that route by studying the fluid phase behavior of hazardous chemicals which are produced on a large scale, mostly as intermediates. The investigated molecules are Ethylene oxide, Ethylene glycol and Water.

All three molecules are of high industrial relevance. The production of Ethylene oxide and its further hydration to Ethylene glycol is a difficult task due to the reactivity and hazardous nature of Ethylene oxide.⁶ As Ethylene oxide almost immediately reacts with water, experimental investigations are nearly impossible. Here, molecular modeling and simulation helps to understand the fluid phase behavior of the regarded components for the use in process optimization. Further details about the individual systems are given below.

For the latter two pure substances, new force fields were developed here. Both were optimized to experimental data on vapor pressure and saturated liquid density. In the case of Ethylene glycol, results from quantum chemical (QC) calculations were taken into account as well. Knowledge on vapor-liquid equilibria (VLE) of the binary mixtures of those compounds is crucial for the design and optimization of thermal separation operations.

Molecular model class

To describe the intermolecular interactions, a varying number of Lennard-Jones (LJ) sites, superimposed point charges and point dipoles was used. Point dipoles were employed for the description of the electrostatic interactions to reduce the computational effort during simulation. However, a point dipole may, e.g. when a simulation program does not support this interaction site type, be approximated by two point charges $\pm q$ separated by a distance l . Limited to small l , this distance may be chosen freely as long as $\mu = ql$ holds. A good choice for l is $\sigma/20$, where σ is the LJ size parameter.⁷

The parameters of the present force fields can be separated into three groups. Firstly, the geometric parameters specify the positions of the different interaction sites. Secondly, the electrostatic parameters define the polar interactions in terms of point charges and dipoles. Finally, the dispersive and repulsive parameters determine the attraction by London forces and the repulsion by overlaps of the electronic orbits. Here, the LJ 12-6 potential^{8,9} was used to allow for a straightforward compatibility with the overwhelming majority of the force fields in the literature.

The total intermolecular interaction energy thus writes as

$$U = \sum_{i=1}^{N-1} \sum_{j=i+1}^N \left\{ \sum_{a=1}^{S_i^{\text{LJ}}} \sum_{b=1}^{S_j^{\text{LJ}}} 4\epsilon_{ijab} \left[\left(\frac{\sigma_{ijab}}{r_{ijab}} \right)^{12} - \left(\frac{\sigma_{ijab}}{r_{ijab}} \right)^6 \right] + \sum_{c=1}^{S_i^e} \sum_{d=1}^{S_j^e} \frac{1}{4\pi\epsilon_0} \left[\frac{q_{ic}q_{jd}}{r_{ijcd}} + \frac{q_{ic}\mu_{jd} + \mu_{ic}q_{jd}}{r_{ijcd}^2} \cdot f_1(\boldsymbol{\omega}_i, \boldsymbol{\omega}_j) + \frac{\mu_{ic}\mu_{jd}}{r_{ijcd}^3} \cdot f_2(\boldsymbol{\omega}_i, \boldsymbol{\omega}_j) \right] \right\}, \quad (1)$$

where r_{ijab} , ϵ_{ijab} , σ_{ijab} are the distance, the LJ energy parameter and the LJ size parameter, respectively, for the pair-wise interaction between LJ site a on molecule i and LJ site b on molecule j . The permittivity of vacuum is ϵ_0 , whereas q_{ic} and μ_{ic} denote the point charge magnitude and the dipole moment of the electrostatic interaction site c on molecule i and so forth. The expressions $f_x(\boldsymbol{\omega}_i, \boldsymbol{\omega}_j)$ stand for the dependency of the electrostatic interactions on the orientations $\boldsymbol{\omega}_i$ and $\boldsymbol{\omega}_j$ of the molecules i and j .^{10,11} Finally, the summation limits N , S_x^{LJ} and S_x^{e} denote the number of molecules, the number of LJ sites and the number of electrostatic sites, respectively.

For a given molecule, i.e. in a pure fluid throughout, the interactions between LJ sites of different type were defined here by applying the standard Lorentz-Berthelot combining rules^{12,13}

$$\sigma_{ijab} = \frac{\sigma_{iiaa} + \sigma_{jjbb}}{2}, \quad (2)$$

and

$$\epsilon_{ijab} = \sqrt{\epsilon_{iiaa}\epsilon_{jjbb}}. \quad (3)$$

Molecular pure substance models

All three molecules studied in the present work do not exhibit significant conformational changes beside Ethylene Glycol. Thus their internal degrees of freedom were neglected and the force fields were chosen to be rigid.

Ethylene oxide

The employed Ethylene oxide model consists of three LJ sites (one for each methylene (CH₂) group and one for the oxygen atom) plus one dipole. It was taken from previous work of our group¹⁴ that was the first entry in the 2007 Industrial Fluid Properties Simulation Challenge.⁴ This model yields mean unsigned errors in vapor pressure, saturated liquid density and enthalpy of vaporization of 1.5 %, 0.4 % and 1.8 %, respectively. This model was assessed with respect to numerous thermophysical properties including transport data. Further details are given in the original publication.¹⁴

Ethylene glycol

Ethylene glycol is an organic compound that is widely used as an automotive antifreeze agent and as a precursor to polymers like Poly(ethylene)terephthalate (PET) and Poly(ethylene)glycol (PEG). At ambient conditions, pure Ethylene glycol in its pure form is an odorless, colorless, syrupy liquid.

Because of this widespread technological interest, different force fields for Ethylene glycol are available in the literature. Most force fields^{15–19} include internal degrees of freedom and were optimized to reproduce properties of the liquid state, e.g. density and enthalpy, only at one given temperature. These force fields are commonly used for biomolecular simulations or for simulations of ionic liquids. Ferrando et al.²⁰ recently developed a flexible force field that was more broadly optimized to thermophysical properties along the vapor-liquid saturation curve.

For modeling Ethylene glycol, its strong hydrogen bonding interactions due to its two hydroxyl groups must be considered. The intermolecular interactions were thus described here by four LJ sites plus six point charges, being located exactly at the positions of the Hydrogen atoms, Oxygen atoms and methylene groups, cf. Figure 1. The geometric structure of the molecule was determined by QC and initially the magnitudes of six point charges were taken from an Ethanol model by Schnabel et al.²¹

A rigid molecular model was assumed for Ethylene glycol, which is a significant simplification, since this molecule may occur in numerous different conformations. This simplification may be on the fringe of a reasonable modeling, but it offers advantages in terms of computational cost. Moreover, it was found for many molecules with a similar size that the VLE properties can be described well with rigid models. However, for other properties, such as transport data, quantitatively correct predictions cannot be expected.

The geometric data of the molecular Ethylene glycol model, i.e. bond lengths, angles and dihedrals, were derived from QC calculations. Therefore, a geometry optimization by energy minimization was initially performed using the QC code GAMESS(US).²² The Hartree-Fock level of theory was applied with a relatively small (6-31G) basis set. The resulting configuration of the

atoms was taken to specify the spatial distribution of the LJ sites. Among the ten most probable conformers,¹⁶ the three lowest minima correspond to one *trans* and two *gauche* forms. Despite the fact that the *gauche* forms are energetically more favorable, the *trans* form was chosen here, because the capability for hydrogen bonding is most pronounced in this case.

The dispersive and repulsive interactions of the Hydrogen atoms were modeled together with the atom they are bonded to. For the methylene united atom site, the LJ potential was located at the geometric mean of the nuclei. This empirical offset follows the work of Ungerer et al.²³ who optimized transferable force fields for n-Alkanes.

It would be highly desirable to also parameterize the dispersive and repulsive LJ interactions using *ab initio* methods as well. However, for an estimation of the dispersive and repulsive interactions at least two molecules must be taken into account. To properly scan the energy hyper surface, many QC calculations at different distances and orientations of the molecules have to be performed. As the dispersive, and partly also the repulsive, interactions are usually only a very small fraction of the total energy that results from QC, highly accurate methods like coupled cluster (CC) with large basis sets or even extrapolations to the basis set limit must be employed for this task.²⁴

Due to the fact that this is computationally too expensive for engineering purposes, LJ parameters for a given atom or molecular group were initially passed on from other force fields. Some of these parameters were subsequently fitted in an optimization process to yield accurate VLE data.

The optimization was done with a Newton scheme following Stoll.^{25,26} The applied method has similarities with the one published by Ungerer et al.²⁷ It relies on a least-square minimization of a weighted fitness function that quantifies the deviations of simulation results for a given force field from experimental reference data.

Correlations of experimental data for vapor pressure, saturated liquid density and enthalpy of vaporization, taken from the DIPPR database,²⁸ were used as reference data for model adjustment and evaluation. The quantitative comparison between simulation results and correlations was done by applying fits to the simulation data according to Lotfi et al.²⁹ The relative deviation between

fit and correlation was calculated in steps of 1 K in the temperature range where simulations were performed and is denoted by "mean unsigned error" in the following.

VLE were determined by molecular simulation with the Grand Equilibrium method,³⁰ the technical details are given in the appendix. The optimized parameter set of the new Ethylene glycol model is summarized in Table 1. The pure substance VLE simulation results obtained with the new model are shown in absolute terms in Figure 2 to Figure 4, where they are compared to the DIPPR correlations. Numerical simulation results for vapor pressure, saturated densities and enthalpy of vaporization are given in Table 2. The critical properties were determined through fits to the present VLE simulation results as suggested by Lotfi et al.²⁹ The estimated uncertainties of critical temperature, critical density and critical pressure from simulation are 1, 3 and 3 %, respectively. Table 3 compares these critical properties to experimental data.^{14,31–37} An excellent agreement was achieved, which is almost throughout within the combined error bars.

Figure 5 shows the deviation plots, based on the DIPPR correlations, of the present simulation data and the simulation data by Ferrando et al.²⁰ Furthermore, four sets of experimental data^{31–34} are included. A good agreement was obtained for the present model, yielding mean unsigned errors for vapor pressure, saturated liquid density and enthalpy of vaporization of 4.8, 0.8 and 13.4 %, respectively, in the temperature range from 300 to 700 K, which is about 42 to 97 % of the critical temperature. Compared to the model by Ferrando et al.,²⁰ the present model shows significant improvements in the description of the saturated liquid density and the vapor pressure. For the enthalpy of vaporization, the model by Ferrando et al.²⁰ shows a better performance. Both for vapor pressure and saturated liquid density, the simulation data show larger relative deviations at low temperatures. As usual, the vapor pressure from simulation shows larger statistical uncertainties at low temperatures. For the enthalpy of vaporization, a significant and almost constant offset is present.

For the other force fields from the literature^{15,16,18,19} no VLE data was found. However, Sze-
fczyk and Cordeiro¹⁹ compared their force field to some other models from the literature for the liquid state point at 298 K and 1 bar. Table 4 compares the present force field to the OPLS-AA

model by Jorgensen et al.,^{38,39} a modified OPLS-AA model by Kony et al.,¹⁷ a force field by Gubskaya and Kusalik,¹⁵ the force field by Szczyk and Cordeiro¹⁹ and to experimental data.^{28,40,41} Compared with the other models, the present molecular performs best for the volume expansivity, second best for both the isothermal compressibility and enthalpy of vaporization, and third best for the density. In general, despite the fact that the internal degrees of freedom were neglected, the performance of the present force field is very satisfying as it well describes the VLE properties over a wide temperature range and is also capable to quantitatively predict thermodynamic properties of the liquid which were not used for the model adjustment.

In Figure 6, the pair correlation functions of Ethylene glycol at 298 K and 1 bar are presented for the oxygen-oxygen (OO), carbon-oxygen (CO) and carbon-carbon (CC) site-site distances. The first peaks are at 2.85, 3.6 and 3.8 Å, respectively. The OO peak is in very good agreement with experimental neutron diffraction data (2.8 Å).⁴² The CO and CC peaks are in good to fair agreement with the simulation results by Oliveira and Freitas,¹⁶ who predicted 3.5 and 4.36 Å. Please note, that the CC peak position of the present work is not straightforward comparable with the results by Oliveira and Freitas,¹⁶ due to the fact that the united atom approach was used here that comprises the carbon atom and two hydrogen atoms.

Water

Since the early nineteen sixties, numerous force fields for Water were developed and investigated regarding their capability to describe the thermophysical and the structural fluid properties qualitatively and quantitatively. Many different potential types have been used and the number of available models is vast. Guillot⁴³ reported a survey on Water models which contain rigid, flexible, dissociable and polarizable interaction sites. Further reviews on Water models are given by Brodsky,⁴⁴ Wallqvist and Mountain,⁴⁵ Finney⁴⁶ and Vega and Abascal.⁴⁷

None of the force fields reviewed by these authors⁴³⁻⁴⁷ satisfactorily covers the properties of Water over the complete technically relevant range of fluid states. Most of them favorably describe the thermophysical properties only close to the state points to which they were adjusted, i.e. often

close to ambient conditions. Only some of them yield fair predictions at state points far away from the adjustment region.

Recently, Paricaud et al.⁴⁸ proposed a rather complex force field which covers the properties of water from dimer to condensed phases at extreme conditions accurately. It describes vapor pressure, saturated liquid density and heat of vaporization for temperatures between 331 and 610 K with mean unsigned errors of 11.3 %, 1.4 % and 3.9 %, respectively. To our knowledge, this is the most accurate representation of the VLE properties on the basis of a force field with state-independent parameters so far. However, the model of Paricaud et al.⁴⁸ is based on Gaussian charge polarizable interaction sites, i.e. smeared out charges to describe electrostatics and hydrogen bonding. Additionally, it uses one Buckingham exponential-6 site⁴⁹ to consider repulsion and dispersion. Thus, this Water model is computationally expensive and not straightforwardly compatible with the overwhelming majority of LJ-based force fields from the literature for simulations of mixtures.

To investigate whether a much simpler force field can describe the VLE properties of Water with a similar quality as the model of Paricaud et al.,⁴⁸ the rigid four-site TIP4P model type, as proposed by Jorgensen et al.,⁵⁰ was studied here. This model type consists of three point charges, excentrically superimposed to one LJ site, cf. Figure 7. The two positive point charges represent the Hydrogen atoms, the negative point charge is located at the bisection of the Hydrogen sites. The LJ site is located at the Oxygen atom such that all sites are situated in a plane.

Recently, the TIP4P model was re-parameterized by Horn et al.⁵¹ (TIP4P-Ew). Two further optimizations for the TIP4P model type were recently suggested by Abascal and Vega⁵² (TIP4P/2005) and Abascal et al.⁵³ (TIP4P/Ice). Furthermore, a TIP4P-like model was developed by Berendsen et al.⁵⁴ (SPC/E). Among these models, for TIP4P/Ice no VLE data are available, thus it is not discussed in the following.

The parameters of the TIP4P, TIP4P-Ew, TIP4P/2005, TIP4P/Ice, SPC/E as well as of the present model are given in Table 5. The distance between the Oxygen atom and the Hydrogen atoms in a water molecule is 0.95718 Å.⁵⁵ Thus most of the TIP4P type models adopt the value 0.9572 Å. However, this distance was chosen to be 40 % larger for the present model. This ex-

tended bond length was chosen to achieve a more localized hydrogen bonding. However, the magnitude of the point charges of the present model was chosen to be smaller than that of other TIP4P type models and the attractive force was compensated by a relatively high LJ energy parameter ϵ .

By choosing this extended bond length, which does not correspond to the physical nature of the molecule, it was possible to achieve a superior performance in describing the VLE. It is thus a tradeoff between the highest possible resolution for the sake of the big picture at reasonable computational cost.

Figure 8 shows the deviation plots, where also simulation results of the TIP4P model by Lísal et al.,⁵⁶ the SPC/E model by Guissani and Guillot,⁵⁷ the TIP4P/2005 model by Vega et al.,⁵⁸ the TIP4P-Ew model by Baranyai et al.⁵⁹ as well as several sets of experimental data^{35–37} are included. A very good agreement was obtained for the present model, yielding mean unsigned errors for vapor pressure, saturated liquid density and enthalpy of vaporization of 7.2, 1.1 and 2.8 %, respectively, in the temperature range from 300 to 600 K, which is about 46 to 93 % of the critical temperature. Among the five force fields, TIP4P/2005 has the best performance for the saturated liquid density at low temperatures, but at higher temperatures, the deviations increase. However, it performs poorest for the vapor pressure (from 25 up to 80 %) and also the enthalpy of vaporization exhibits a large deviation at 298 K. The original TIP4P model shows the largest deviations for both saturated liquid density and enthalpy of vaporization. TIP4P-Ew and SPC/E have an average performance for all three properties. SPC/E shows similar deviations as TIP4P/2005 for the enthalpy of vaporization.

Although the main goal for the development of the present water model was the accurate description of the VLE, predictions on the structure of liquid water are provided in terms of the radial distribution function for the oxygen-oxygen (OO) distance at 298 K and 1 bar in Figure 9. The present model predicts the first peak at 3 Å which is at a somewhat larger distance than the experimental data with around 2.8 Å as reported by Soper.⁶⁰ The magnitude of the peak is in good agreement with the data by Soper.⁶⁰ Also for the remaining extrema, the present results are at somewhat larger distances.

Second virial coefficient

For Ethylene oxide and Water, second virial coefficient data from experimental work are available.^{61,62} For Ethylene glycol, only predictions by Abusleme and Vera⁶³ are available. Figure 10 compares the predictions based on the present force fields with these data. The agreement is very good for Ethylene oxide and Water. At high temperatures, the Ethylene glycol model yields significantly different results than the group contribution method by Abusleme and Vera.⁶³ These could be attributed to the rigid nature of the force field, which does not cover the conformational changes that play an increasing role under these conditions.

Molecular mixture models

On the basis of pairwise additive pure fluid models, molecular modeling of mixtures reduces to specifying the interactions between unlike molecules. Unlike interactions consist of two different types here. The unlike electrostatic interactions, e.g. between charges as well as between charge and dipole, were treated in a physically straightforward way, simply using the laws of electrostatics.

Unfortunately, the treatment of the unlike dispersive attraction is not straightforward. If a mixture A + B is modeled on the basis of LJ sites, the knowledge of the unlike LJ parameters σ_{AB} and ϵ_{AB} is required. Due to the fact that there is no sound physical framework for the determination of these parameters, the broadly used Lorentz-Berthelot combining rules are the usual starting point⁶⁴ with

$$\sigma_{AB} = (\sigma_A + \sigma_B)/2, \quad (4)$$

and

$$\epsilon_{AB} = \sqrt{\epsilon_A \epsilon_B}. \quad (5)$$

Applying σ_{AB} and ϵ_{AB} as given by Eq. (4) and Eq. (5) allows for the prediction of mixture properties from pure fluid data alone.^{25,64–67} But as shown in these publications, a significant improvement can be achieved by introducing one state independent binary parameter ξ to adjust the unlike

energy parameter

$$\varepsilon_{AB} = \xi \sqrt{\varepsilon_A \varepsilon_B}. \quad (6)$$

It should be pointed out that A and B are molecule species that may each be described by several LJ sites with different energy parameters ε . Thus ξ is a single overall parameter that acts consistently on all individual unlike LJ interactions of the pair A + B.

For VLE, it was shown in Ref.⁶⁴ that ξ can be adjusted to a single experimental binary vapor pressure. Specifying temperature and saturated liquid composition, ξ has hardly any influence on the saturated liquid density and a minor influence on the saturated vapor composition. The benefit of ξ lies in an significantly enhanced representation of the two-phase envelope. The binary parameter was adjusted here following the same procedure as in prior work of our group.^{25,66,67}

Table 6 lists the state point (i.e. temperature T and saturated liquid mole fraction of the lower boiling component x_A) and the experimental vapor pressure p^{exp} which was used for the adjustment as well as the resulting binary parameter ξ . For direct comparison and validation, a VLE simulation with the adjusted mixture model was performed at this state point. The resulting vapor pressure p and saturated vapor composition y_A from simulation are also listed in Table 6 and can there numerically be compared to experimental vapor pressure data.

Binary vapor-liquid equilibria

Based on the three pure substance models presented above, VLE data were predicted for all three binary combinations. Their phase behavior is throughout zeotropic. Full numerical VLE simulation data are given in Table 7, which also contains the saturated densities and the heat of vaporization from simulation. Because the saturated densities and the heat of vaporization from experiment are not available for comparison, they are not further discussed here.

For orientation and comparison, the results of the Peng-Robinson equation of state (EOS)⁶⁸ with adjusted binary parameter k_{ij} are also shown. A definition of the binary parameter k_{ij} is given in the appendix. The EOS was optimized to the experimental vapor pressure at the same state point

as the molecular mixture model.

Ethylene oxide + Water

Figure 11 shows isobaric VLE of Ethylene oxide + Water at 0.4428 MPa from experiment, simulation and Peng-Robinson EOS. Figure 12 presents isothermal VLE at the temperatures 350 and 370 K. The binary parameters $\xi = 1.126$ and $k_{ij} = -0.1$ were adjusted to the vapor pressure measured by Schilk and Hurd⁶⁹ at 370 K for a liquid mole fraction $x_{EO} = 0.03$ mol/mol. Both $\xi = 1.126$ and $k_{ij} = -0.1$ differ quite strongly from the values $\xi = 1$ and $k_{ij} = 0$ that would be used in a strictly predictive application. However, particularly the interactions of water are dominated by electrostatics so that the comparably weak unlike dispersive interaction has to be modified quite significantly to adjust the mixture model.

At 0.4428 MPa, the mixture is sub-critical, the phase envelope is wide with a concave bubble line and a slightly convex dew line, cf. Figure 11. The simulation points show a very good agreement with the experimental data, but the Peng-Robinson EOS matches only on the saturated liquid line, i.e. it fails to describe the saturated vapor line outside the Water-rich area. Due to the shortage of isothermal experimental data, six points were interpolated from the experimental data by Schilk and Hurd⁶⁹ to form the two isothermal data sets in Figure 12. There, the simulation results disagree with Peng-Robinson EOS outside of the Water-rich region.

Figure 13 shows the present simulation results for the Henry's law constant of Ethylene oxide in Water, which is a property that is technically particularly important, e.g. for hazard and operability studies. As no experimental data were found in the literature, no comparison can be made. To our knowledge, the simulation data reported here (cf. Table 8) are therefore the first published data on the Henry's law constant of Ethylene oxide in Water. Another important property, which is experimentally practically inaccessible, can be obtained from that data. It is the enthalpy of absorption of Ethylene oxide in Water in the absence of the chemical reactions of those substances. It can be obtained either from the temperature dependence of the Henry's law constant⁷⁰ shown in Figure 13 or directly from simulations at infinite dilution.⁷¹ The results are consistent with -15

(± 5) kJ/mol and -21 (± 1) kJ/mol, respectively, and are almost independent on the temperature. The number in parentheses is the uncertainty of the enthalpy of absorption.

Ethylene oxide + Ethylene glycol

Figure 14 shows isothermal VLE data of Ethylene oxide + Ethylene glycol at 378.15 and 360.15 K from experiment, simulation and Peng-Robinson EOS. The mixture is sub-critical for these temperatures and the phase envelope, according to the Peng-Robinson EOS, is very wide with a S-shaped saturated liquid line and a concave saturated vapor line.

The binary parameters $\xi = 1.016$ and $k_{ij} = 0.01$ were adjusted to the vapor pressure measured by Di Serio et al.⁷² at 378.15 K and $x_{EO} = 0.1$ mol/mol. The present simulation results are in good agreement with the experimental data set by Di Serio et al.⁷² As shown in Figure 14, experimental data are only available at low Ethylene oxide concentrations (≤ 0.1 mol/mol). The present molecular simulations indicate that at higher Ethylene oxide concentrations, a small miscibility gap may exist near the equimolar composition.

Water + Ethylene glycol

Isothermal VLE data of Water + Ethylene glycol from experiment, simulation and Peng-Robinson EOS are presented in Figure 15 at 383.15 and 395.15 K. For both temperatures, the mixture is sub-critical and the phase envelope is wide with a slightly concave saturated liquid line. The experimental vapor pressure measured by Lancia et al.⁷³ at 395.15 K and $x_{H_2O} = 0.466$ mol/mol was taken for the optimization of the mixture models, yielding $\xi = 0.8$ and $k_{ij} = -0.066$. Even with the optimization, it was not possible to describe the experimental data by Lancia et al.⁷³ very well. A further decrease of the ξ value did not improve the description of the VLE, in fact the opposite effect occurred. Maximum deviations of around 60 % in terms of the vapor pressure of the mixture between simulation results and experimental data were found at low Water mole fractions. For higher Water mole fractions, the average deviations are around 30 %. We assume that these unfavorable findings are related to the fact that Ethylene glycol was modeled neglecting

the internal degrees of freedom, which may be too crude when details of its interactions with water are of interest.

At 395.15 K, the Peng-Robinson EOS fails to describe the saturated liquid line in the Ethylene glycol-rich region and it does not match well with saturated vapor line either. Regarding the isotherm 383.15 K, it can be seen that the binary parameter k_{ij} of the Peng-Robinson EOS should be assumed to be temperature dependent.

Henry's law constant of Ethylene oxide in liquid mixtures of Water + Ethylene glycol

The solubility of Ethylene oxide in mixtures of Water and Ethylene glycol is important for the industrial production of Ethylene glycol from Ethylene oxide and Water.⁶ Despite this importance, data on the solubility of Ethylene oxide in mixtures of Water and Ethylene glycol are not available in the literature. This is related to the high reactivity of Ethylene oxide, which makes such measurements difficult. Another problem is that, at least at higher temperatures, Ethylene oxide will always react with water so that the physical solubility of Ethylene oxide cannot be measured directly. However, it is the central property needed for modeling the thermophysical data in the studied systems and, hence, it forms a basis for process simulation. Molecular simulations provide an unique opportunity for obtaining the physical solubility of Ethylene oxide in aqueous solutions.

Figure 16 shows the Henry's law constant of Ethylene oxide in liquid mixtures of Water + Ethylene glycol in dependence of the Ethylene glycol mole fraction (calculated on a Ethylene oxide free basis) at 350 and 500 K. Numerical simulation data are presented in Table 8. The Ethylene oxide and Ethylene glycol mole fractions correspond to Ethylene oxide free mass ratios of Water + Ethylene glycol of 1:3, 1:4, 1:6 and 1:10. At 350 K, hardly any significant influence upon adding Ethylene glycol to the solvent Water on the Henry's law constant of Ethylene oxide was found. The large statistical uncertainties due to the low temperature render a discussion of these results difficult. At 500 K, the Henry's law constant of Ethylene oxide slightly decreases with rising

Ethylene glycol mole fraction. Like for Ethylene oxide in Water, the enthalpy of absorption can be calculated from the temperature dependence as well as directly from the energies obtained by molecular simulation. The results from the present study indicate that the enthalpy of absorption of Ethylene glycol does not depend on the addition of Ethylene glycol to the solvent Water.

It should be noted, however, that these predictions may be less reliable than, e.g. the ones for the solubility of Ethylene oxide in pure Water. The shortcomings observed for the predictions in the system Ethylene glycol + Water, presumably due to the neglect of the internal degrees of freedom of Ethylene glycol, may also have consequences here as well.

Conclusion

Molecular modeling and simulation was applied to predict VLE of binary mixtures containing Ethylene oxide, Ethylene glycol and Water. New force fields were developed for Ethylene glycol and Water, partly based on quantum chemical information on molecular geometry and electrostatics. Furthermore, experimental data on the vapor pressure and the saturated liquid density were taken into account to optimize the pure substance models. These properties were accurately represented from the triple point to the critical point. Critical values of temperature, density and pressure from present simulations agree with experimental data within the combined error bars. The new models were compared with models from the literature with respect to their representation of the VLE properties. In addition, the second virial coefficient was predicted for Ethylene oxide, Ethylene glycol and Water. Overall, the comparison with experimental data is favorable.

All binary mixtures of these three components were simulated, where one state independent parameter was adjusted to one experimental state point. For the binary mixtures Ethylene oxide + Water and Ethylene oxide + Ethylene glycol, a good agreement was found between experiment and molecular simulation. For Water + Ethylene glycol, molecular simulation underpredicts the vapor pressure of the mixture. This may be related to the neglect of the internal degrees of freedom in the present Ethylene glycol model.

Henry's law constant data of Ethylene oxide in liquid mixtures of Ethylene glycol + Water were predicted at 350 and 500 K. At 350 K, no significant influence of the liquid composition was found, whereas at 500 K, the Henry's law constant of Ethylene oxide slightly decreases with rising Ethylene glycol mole fraction in the liquid mixture. The enthalpy of absorption of Ethylene oxide in these mixtures does not depend strongly on the temperature or composition and is about -15 (± 5) kJ/mol and -21 (± 1) kJ/mol, respectively. To our knowledge, this is the first time that values for the physical solubility of Ethylene oxide (no chemical reactions with Water or Ethylene glycol) are reported.

Acknowledgement

We gratefully acknowledge Deutsche Forschungsgemeinschaft "TFB 66" and BASF SE for funding this project. The presented research was conducted under the auspices of the Boltzmann-Zuse Society of Computational Molecular Engineering (BZS), and the simulations were performed on the national super computer NEC SX-8 at the High Performance Computing Center Stuttgart (HLRS) and on the HP X6000 super computer at the Steinbuch Centre for Computing, Karlsruhe.

We would like to thank Xijun Fu, Tianmin Du and Shan Yuan for handling numerous simulation runs and helping to prepare the material for publication.

Appendix: Simulation details

The Grand Equilibrium method³⁰ was used to calculate VLE data. Monte Carlo simulations were performed in the NpT ensemble for the liquid. Thereby, the chemical potential was calculated by the gradual insertion method.^{74,75} The number of molecules was 500. Starting from a face centered cubic lattice, 15 000 Monte Carlo cycles were performed for equilibration and 50 000 for production, each cycle containing 500 translation moves, 500 rotation moves, and 1 volume move. Every 50 cycles, 5000 fluctuating state change moves, 5000 fluctuating particle translation/rotation moves, and 25000 biased particle translation/rotation moves were performed, to determine the

chemical potential. These yield the chemical potential in dense and strong interacting liquids with high accuracy, leading to reasonable uncertainties in the VLE.

For the corresponding vapor, Monte Carlo simulations in the pseudo- μVT ensemble were performed. The simulation volume was adjusted to lead to an average number of 500 molecules in the vapor phase. After 2 000 initial NVT Monte Carlo cycles, starting from a face centered cubic lattice, 10 000 equilibration cycles in the pseudo- μVT ensemble were performed. The length of the production run was 50 000 cycles. One cycle is defined here to be a number of attempts to displace and rotate molecules equal to the actual number of molecules plus three insertion and three deletion attempts.

The cut-off radius was set to 17.5 Å throughout and a center of mass cut-off scheme was employed. Lennard-Jones long-range interactions beyond the cut-off radius were corrected employing angle averaging as proposed by Lustig.⁷⁶ Electrostatic interactions were approximated by an effective molecular dipole and corrected using the reaction field method.¹⁰ Statistical uncertainties of the simulated values were estimated by a block averaging method.⁷⁷

All simulations were carried out with the molecular simulation tool *ms2*.⁷⁸

The adjustable binary parameter k_{ij} of the following mixing rules

$$a_{ij} = \sqrt{a_{ii}a_{jj}}(1 - k_{ij}). \quad (7)$$

and

$$b_{ij} = (b_{ii} + b_{jj})/2, \quad (8)$$

where a_{ij} and b_{ij} are the cross parameters of the one-fluid mixing rule of van der Waals used in the Peng-Robinson EOS.⁶⁸

Literature Cited

- (1) Case, F.; Chaka, A.; Friend, D. G.; Frurip, D.; Golab, J.; Johnson, R.; Moore, J.; Mountain, R. D.; Olson, J.; Schiller, M.; Storer, J. The first industrial fluid properties simulation challenge. *Fluid Phase Equilib.* **2004**, *217*, 1–10.
- (2) Case, F.; Chaka, A.; Friend, D. G.; Frurip, D.; Golab, J.; Gordon, P.; Johnson, R.; Kolar, P.; Moore, J.; Mountain, R. D.; Olson, J.; Ross, R.; Schiller, M. The second industrial fluid properties simulation challenge. *Fluid Phase Equilib.* **2005**, *236*, 1–14.
- (3) Case, F. H.; Brennan, J.; Chaka, A.; Dobbs, K. D.; Friend, D. G.; Frurip, D.; Gordon, P. A.; Moore, J.; Mountain, R. D.; Olson, J.; Ross, R. B.; Schiller, M.; Shen, V. K. The third industrial fluid properties simulation challenge. *Fluid Phase Equilib.* **2007**, *260*, 153–163.
- (4) Case, F. H.; Brennan, J.; Chaka, A.; Dobbs, K. D.; Friend, D. G.; Gordon, P. A.; Moore, J. D.; Mountain, R. D.; Olson, J. D.; Ross, R. B.; Schiller, M.; Shen, V. K.; Stahlberg, E. A. The fourth industrial fluid properties simulation challenge. *Fluid Phase Equilib.* **2008**, *274*, 2–9.
- (5) Case, F. H.; Chaka, A.; Moore, J. D.; Mountain, R. D.; Olson, J. D.; Ross, R. B.; Schiller, M.; Shen, V. K.; Stahlberg, E. A. The fifth industrial fluid properties simulation challenge. *Fluid Phase Equilib.* **2009**, *285*, 1–3.
- (6) Weissermel, K.; Arpe, H.-J. *Industrial Organic Chemistry*; VCH Press, Weinheim, 1997.
- (7) Engin, C.; Vrabc, J.; Hasse, H. On the difference between a point quadrupole and an equivalent arrangement of three point charges in force field models for vapor-liquid equilibria. *Mol. Phys.* **2011**, *109*, 1975–1982.
- (8) Jones, J. E. On the Determination of Molecular Fields. I. From the Variation of the Viscosity of a Gas with Temperature. *Proc. Roy. Soc.* **1924**, *106A*, 441–462.
- (9) Jones, J. E. On the Determination of Molecular Fields. II. From the Equation of State of a Gas. *Proc. Roy. Soc.* **1924**, *106A*, 463–477.

- (10) Allen, M. P.; Tildesley, D. J. *Computer simulations of liquids*; Clarendon Press: Oxford, 1987.
- (11) Gray, C. G.; Gubbins, K. E. *Theory of molecular fluids. 1. Fundamentals*; Clarendon Press: Oxford, 1984.
- (12) Lorentz, H. A. Über die Anwendung des Satzes vom Virial in der kinetischen Theorie der Gase. *Ann. d. Phys.* **1881**, *12*, 127–136.
- (13) Berthelot, D. Sur le Mélange des Gaz. *Compt. Rend. Ac. Sc.* **1898**, *126*, 1703–1706.
- (14) Eckl, B.; Vrabec, J.; Hasse, H. On the Application of Force Fields for Predicting a Wide Variety of Properties: Ethylene Oxide as an Example. *Fluid Phase Equilib.* **2008**, *274*, 16–26.
- (15) Gubskaya, A. V.; Kusalik, P. G. Molecular Dynamics Simulation Study of Ethylene Glycol, Ethylenediamine, and 2-Aminoethanol. 1. The Local Structure in Pure Liquids. *J. Phys. Chem. A* **2004**, *108*, 7151–7164.
- (16) Oliveira, O. V.; Freitas, L. C. G. Molecular dynamics simulation of liquid ethylene glycol and its aqueous solution. *J. Mol. Struct. THEOCHEM* **2005**, *728*, 179–187.
- (17) Kony, D.; Damm, W.; Stoll, S.; van Gunsteren, W. F. An improved OPLS-AA force field for carbohydrates. *J. Comp. Chem.* **2002**, *23*, 1416–1429.
- (18) Geerke, D. P.; van Gunsteren, W. F. The performance of non-polarizable and polarizable force-field parameter sets for ethylene glycol in molecular dynamics simulations of the pure liquid and its aqueous mixtures. *Mol. Phys.* **2007**, *105*, 1861–1881.
- (19) Szcfczyk, B.; Cordeiro, M. N. D. S. Physical Properties at the Base for the Development of an All-Atom Force Field for Ethylene Glycol. *J. Phys. Chem. B* **2011**, *115*, 3013–3019.
- (20) Ferrando, N.; Lachet, V.; Teuler, J.-M.; Boutin, A. Transferable Force Field for Alcohols and Polyalcohols. *J. Phys. Chem. B* **2009**, *113*, 5985–5995.

- (21) Schnabel, T.; Vrabc, J.; Hasse, H. Henry's Law Constants of Methane, Nitrogen, Oxygen and Carbon Dioxide in Ethanol from 273 to 498 K: Prediction from Molecular Simulation. *Fluid Phase Equilib.* **2005**, *233*, 134–143.
- (22) Schmidt, M. W.; Baldrige, K. K.; Boatz, J. A.; Elbert, S. T.; Gordon, M. S.; Jensen, J. H.; Koseki, S.; Matsunaga, N.; Nguyen, K. A.; Su, S.; Windus, T. L.; Dupuis, M.; Montgomery, J. A. General atomic and molecular electronic structure system. *J. Comput. Chem.* **1993**, *14*, 1347–1363.
- (23) Ungerer, P.; Beauvais, C.; Delhommelle, J.; Boutin, A.; Rousseau, B.; Fuchs, A. H. Optimization of the anisotropic united atoms intermolecular potential for n-alkanes. *J. Chem. Phys.* **2000**, *112*, 5499–5510.
- (24) Sandler, S. I.; Castier, M. Computational quantum mechanics: An underutilized tool in thermodynamics. *Pure Appl. Chem.* **2007**, *79*, 1345–1359.
- (25) Stoll, J. In *Molecular Models for the Prediction of Thermophysical Properties of Pure Fluids and Mixtures*; VDI, F.-B., Ed.; Reihe 3; VDI-Verlag: Düsseldorf, 2005.
- (26) Eckl, B.; Vrabc, J.; Hasse, H. Set of molecular models based on quantum mechanical ab initio calculations and thermodynamic data. *J. Phys. Chem. B* **2008**, *112*, 12710–12721.
- (27) Ungerer, P.; Boutin, A.; Fuchs, A. H. Direct calculation of bubble points by Monte Carlo simulation. *Mol. Phys.* **1999**, *97*, 523–539.
- (28) Rowley, R. L.; Wilding, W. V.; Oscarson, J. L.; Yang, Y.; Zundel, N. A.; Daubert, T. E.; Danner, R. P. *DIPPR[®] Data Compilation of Pure Compound Properties*; Design Institute for Physical Properties, AIChE, New York, 2006.
- (29) Lotfi, A.; Vrabc, J.; Fischer, J. Vapour liquid equilibria of the Lennard-Jones fluid from the NpT plus test particle method. *Mol. Phys.* **1992**, *76*, 1319–1333.

- (30) Vrabec, J.; Hasse, H. Grand Equilibrium: vapour-liquid equilibria by a new molecular simulation method. *Mol. Phys.* **2002**, *100*, 3375–3383.
- (31) Marchetti, A.; Preti, C.; Tagliazucchi, M.; Tassi, L.; Tosi, G. The N,N-Dimethylformamide/Ethane-1,2-diol Solvent System. Density, Viscosity and Excess Molar Volume at Various Temperatures. *J. Chem. Eng. Data* **1991**, *36*, 360–365.
- (32) Ambrose, D.; Hall, D. J. Thermodynamic Properties of Organic Oxygen Compounds. L. The Vapour Pressures of 1,2-Ethanediol (Ethylene Glycol) and bis(2-Hydroxyethyl) ether (Diethylene Glycol). *J. Chem. Thermodyn.* **1981**, *13*, 61–66.
- (33) Salvi, M. V.; Van Hook, W. A. Isotope Effects on PVT Properties of Ethylene Glycols (C₂H₂OH)₂ and (CH₂OD)₂. Pressure and Isotope Dependence of Liquid-liquid Phase Separation of (CH₂OH)₂/CH₃NO₂ and (CH₂OD)₂/CH₃NO₂ Solutions. *J. Phys. Chem.* **1990**, *94*, 7812–7820.
- (34) Curme, G. O.; Johnson, F. *Glycol: Physical Properties of Ethylene Glycol*; Reinhold Publishing: New York, 1952.
- (35) American Petroleum Institute Research Project 44, Selected Values of Properties of Hydrocarbons and Related Compounds, Thermodynamic Research Center, Texas A&M University, College Station, Texas (1980).
- (36) Haar, L.; Gallagher, J. S.; Kell, G. S. *NBS/NRC Steam Tables. Thermodynamic and Transport Properties and Computer Programs for Vapor and Liquid States of Water in SI Units*; Hemisphere Publishing: Washington, 1984.
- (37) Keenan, J. H.; Keyes, F. G.; Hill, P. G.; Moore, J. G. *Steam Tables. Thermodynamic Properties of Water Including Vapor, Liquid, and Solid Phases*; John Wiley & Sons: New York, 1969.

- (38) Jorgensen, W. L. Optimized intermolecular potential functions for liquid alcohols. *J. Phys. Chem.* **1986**, *90*, 1276–1284.
- (39) Jorgensen, W. L.; Maxwell, D. S.; J., T.-R. Development and Testing of the OPLS All-Atom Force Field on Conformational Energetics and Properties of Organic Liquids. *J. Am. Chem. Soc.* **1997**, *118*, 11225–11236.
- (40) Rodnikova, M. N.; Chumaevskii, N. A.; Troitskii, V. M.; B., K. D. Structure of liquid ethylene glycol. *Rus. J. Phys. Chem.* **2006**, *80*, 826–830.
- (41) Huo, J.-Y.; Battistel, E.; Lumry, R.; Villeneuve, G.; Lavallee, J.-F.; Anusiem, A.; C., J. A comprehensive thermodynamic investigation of water-ethylene glycol mixtures at 5, 25, and 45C. *J. Sol. Chem.* **1988**, *17*, 601–636.
- (42) Bakó, I.; Gróaz, T.; Pálinkás, G. Ethylene glycol dimers in the liquid phase: A study by x-ray and neutron diffraction. *J. Chem. Phys.* **2003**, *118*, 3215–3221.
- (43) Guillot, B. A reappraisal of what we have learnt during three decades of computer simulations on water. *J. Mol. Liq.* **2002**, *101*, 219–260.
- (44) Brodsky, A. Is there predictive value in water computer simulations? *Chem. Phys. Lett.* **1996**, *261*, 563–568.
- (45) Wallqvist, A.; Mountain, R. D. Molecular models of water: Derivation and description. *Rev. Comp. Chem.* **1999**, *13*, 183–247.
- (46) Finney, J. L. The water molecule and its interactions: the interaction between theory, modelling, and experiment. *J. Mol. Liq.* **2001**, *90*, 303–312.
- (47) Vega, C.; Abascal, J. L. F. Simulating water with rigid non polarizable models: a general perspective. *Phys. Chem. Chem. Phys.* **2011**, *13*, 19663–19688.

- (48) Paricaud, P.; Předota, M.; Chialvo, A. A.; Cummings, P. T. From dimer to condensed phases at extreme conditions: Accurate predictions of the properties of water by Gaussian charge polarizable model. *J. Chem. Phys.* **2005**, *122*, 244511–244524.
- (49) Buckingham, R. A. The classical equation of state of gaseous helium, neon and argon. *Proc. Roy. Soc.* **1938**, *168A*, 264–283.
- (50) Jorgensen, W. L.; Chandrasekhar, J. D.; Madura, R. W.; Impey, R. W.; Klein, M. L. Comparison of simple potential functions for simulating liquid water. *J. Chem. Phys.* **1983**, *79*, 926–935.
- (51) Horn, H. W.; Swope, W. C.; Pitner, J. W.; Madura, J. D.; Dick, T. J.; Hura, G. L.; Head-Gordon, T. Development of an improved four-site water model for biomolecular simulations: TIP4P-Ew. *J. Chem. Phys.* **2004**, *120*, 9665–9678.
- (52) Abascal, J. L. F.; Vega, C. A general purpose model for the condensed phases of water: TIP4P/2005. *J. Chem. Phys.* **2005**, *123*, 234505–234516.
- (53) Abascal, J. L. F.; Sanz, E.; García Fernández, R.; Vega, C. A potential model for the study of ices and amorphous water: TIP4P/Ice. *J. Chem. Phys.* **2005**, *122*, 234511–234519.
- (54) Berendsen, H. J. C.; Grigera, J. R.; Straatsma, T. P. The Missing Term in Effective Pair Potentials. *J. Phys. Chem.* **1987**, *91*, 6269–6271.
- (55) Hasted, J. B. *Liquid water: Dielectric properties, in Water A comprehensive treatise*; Plenum Press: New York, 1972.
- (56) Lísal, M.; Smith, W. R.; Nezbeda, I. Accurate vapour-liquid equilibrium calculations for complex systems using the reaction Gibbs Ensemble Monte Carlo simulation method. *Fluid Phase Equilib.* **2001**, *181*, 127–146.
- (57) Guissani, Y.; Guillot, B. A computer simulation study of the liquid-vapor coexistence curve of water. *J. Chem. Phys.* **1993**, *98*, 8221–8235.

- (58) Vega, C.; Abascal, J. L. F.; Nezbeda, I. Vapor-liquid equilibria from the triple point up to the critical point for the new generation of TIP4P-like models: TIP4P/Ew, TIP4P/2005, and TIP4P/ice. *J. Chem. Phys.* **2006**, *125*, 034503.
- (59) Baranyai, A.; Bartók, A.; Chialvo, A. A. Testing the adequacy of simple water models at the opposite ends of the phase diagram. *J. Mol. Liq.* **2007**, *134*, 94–98.
- (60) Soper, A. K. The radial distribution functions of water and ice from 220 to 673 K and at pressures up to 400 MPa. *Chem. Phys.* **2000**, *258*, 121–137.
- (61) Stryjek, R. *Bull. Acad. Pol. Sci. Ser. Sci. Chim.* **1966**, *14*, 307–312.
- (62) Wagner, W.; Pruss, A. The IAPWS Formulation 1995 for the Thermodynamic Properties of Ordinary Water Substance for General and Scientific Use. *J. Phys. Chem. Ref. Data* **2002**, *31*, 387–535.
- (63) Abusleme, J. A.; Vera, J. H. *A Group Contribution Method for Second Virial Coefficients*; The Pennsylvania State University, 1982.
- (64) Schnabel, T.; Vrabec, J.; Hasse, H. Erratum to "‘Henry’s Law Constants of Methane, Nitrogen, Oxygen and Carbon Dioxide in Ethanol from 273 to 498 K: Prediction from Molecular Simulation. Fluid Phase Equilibria, 233:134–143, 2005.'". *Fluid Phase Equilib.* **2006**, *239*, 125–126.
- (65) Carrero-Mantilla, J.; Llano-Restrepo, M. Further Validation of a Set of Quadrupolar Potential Models for Ethylene and Propylene from the Prediction of some Binary Mixture Vapor-Liquid Equilibria by Gibbs-ensemble Molecular Simulation. *Mol. Sim.* **2003**, *29*, 549–554.
- (66) Stoll, J.; Vrabec, J.; Hasse, H. Vapor-Liquid Equilibria of Mixtures Containing Nitrogen, Oxygen, Carbon Dioxide, and Ethane. *AIChE J.* **2003**, *49*, 2187–2198.
- (67) Vrabec, J.; Stoll, J.; Hasse, H. Molecular models of unlike interactions in fluid mixtures. *Mol. Sim.* **2005**, *31*, 215–221.

- (68) Peng, D. Y.; Robinson, D. B. A New Two-Constant Equation of State. *Ind. Chem. Eng. Fundam.* **1976**, *15*, 59–64.
- (69) Schilk, J. A.; Hurd, C. O. Tech. Rep. Rep. No. SHELL 240-57 **1957**, Subject 1896, 11–13.
- (70) Sherwood, A. E.; Prausnitz, J. M. The Heat of Solution of Gases at High Pressure. *AIChE J.* **1962**, *8*, 519–521.
- (71) Chandrasekhar, J.; Jorgensen, W. L. The nature of dilute solutions of sodium ion in water, methanol, and tetrahydrofuran. *J. Chem. Phys.* **1962**, *77*, 5080–5089.
- (72) Di Serio, M.; Tesser, R.; Dimiccoli, A.; Santacesaria, E. Kinetics of Ethoxylation and Propoxylation of Ethylene Glycol Catalyzed by KOH. *Ind. Eng. Chem. Res.* **2002**, *41*, 5196–5206.
- (73) Lancia, A.; Musmarra, D.; Pepe, F. Vapor-liquid equilibria for mixtures of ethylene glycol, propylene glycol, and water between 98 °C and 122 °C. *J. Chem. Eng. Japan* **1996**, *29*, 449–455.
- (74) Vrabc, J.; Kettler, M.; Hasse, H. Chemical potential of quadrupolar two-centre Lennard-Jones fluids by gradual insertion. *Chem. Phys. Lett.* **2002**, *356*, 431–436.
- (75) Nezbeda, I.; Kolafa, J. A New Version of the Insertion Particle Method for Determining the Chemical Potential by Monte Carlo Simulation. *Mol. Sim.* **1991**, *5*, 391–403.
- (76) Lustig, R. Angle-average for the powers of the distance between two separated vectors. *Mol. Phys.* **1988**, *65*, 175–179.
- (77) Flyvbjerg, H.; Petersen, H. G. Error estimates on averages of correlated data. *J. Chem. Phys.* **1989**, *91*, 461–466.
- (78) Deublein, S.; Eckl, B.; Stoll, J.; Lishchuk, S. V.; Guevara-Carrion, G.; Glass, C. W.; Merker, T.; Bernreuther, M.; Hasse, H.; Vrabc, J. ms2: A molecular simulation tool for thermodynamic properties. *Comp. Phys. Commun.* **2011**, *182*, 2350–2367.

Table 1: Parameters of the new molecular model for Ethylene glycol based on Lennard-Jones interaction sites and point charges, cf. Figure 1. The coordinates are given with respect to the center of mass in a principal axes system.

interaction site	x Å	y Å	z Å	σ Å	ϵ/k_B K	q e
OH(1)	1.6941	0.2400	0	3.18	89.31	
OH(2)	-1.6941	-0.2400	0	3.18	89.31	
CH ₂ (1)	-0.4831	0.8857	0	3.50	94.00	
CH ₂ (2)	0.4831	-0.8857	0	3.50	94.00	
point charge at CH ₂ (1)	-0.4831	0.8857	0			0.278
point charge at O(1)	1.6941	0.2400	0			-0.810
point charge at H(1)	-2.4793	0.2072	0			0.532
point charge at CH ₂ (2)	0.4831	-0.8857	0			0.278
point charge at O(2)	-1.6941	-0.2400	0			-0.810
point charge at H(2)	2.4793	-0.2072	0			0.532

Table 2: Vapor-liquid equilibrium simulation results for the pure substances on the basis of the new molecular models. The number in parentheses indicates the statistical uncertainty in the last digit.

T K	p MPa	ρ' mol/l	ρ'' mol/l	Δh_v kJ/mol
Ethylene glycol				
325.00	0.000092 (5)	17.45 (1)	0.000023 (1)	70.24 (7)
350.00	0.00051 (1)	17.18 (1)	0.000111 (3)	69.71 (6)
400.00	0.00722 (6)	16.626 (6)	0.00220 (2)	66.01 (6)
450.00	0.0514 (4)	15.973 (6)	0.0223 (2)	61.17 (4)
500.00	0.2245 (9)	15.218 (6)	0.0458 (2)	56.22 (3)
550.00	0.725 (1)	14.368 (8)	0.1841 (3)	50.09 (3)
600.00	1.78 (1)	13.32 (1)	0.423 (2)	43.44 (4)
650.00	3.73 (2)	12.03 (3)	0.928 (5)	35.31 (6)
700.00	6.78 (3)	10.0 (1)	1.900 (8)	21.2 (2)
Water				
300.00	0.0040 (4)	56.35 (4)	0.00178 (2)	45.41 (1)
320.55	0.0120 (6)	55.23 (3)	0.0045 (2)	44.33 (1)
350.00	0.046 (2)	53.91 (3)	0.0169 (7)	42.86 (1)
373.97	0.109 (3)	52.64 (3)	0.0360 (9)	41.64 (2)
427.40	0.513 (9)	50.06 (4)	0.154 (3)	38.63 (2)
450.00	0.89 (2)	48.85 (5)	0.261 (5)	37.19 (1)
534.25	4.50 (5)	43.10 (5)	1.27 (1)	30.47 (4)
550.00	5.80 (6)	41.75 (7)	1.57 (2)	29.01 (1)
587.67	9.70 (8)	37.8 (2)	2.88 (2)	24.5 (1)
600.00	11.2 (1)	36.3 (2)	3.80 (4)	22.14 (3)

Table 3: Critical properties of the pure substances on the basis of the employed molecular models in comparison to recommended experimental data.

	T_c^{sim}	T_c^{exp}	ρ_c^{sim}	ρ_c^{exp}	p_c^{sim}	p_c^{exp}	Exp.
	K	K	mol/l	mol/l	MPa	MPa	Ref.
Ethylene oxide	469.6	469.15	7.18	7.1278	7.2	7.190	¹⁴
Ethylene glycol	722.0	720.00	5.9	5.92	8.3	8.257	³¹⁻³⁴
Water	649.3	647.10	17.5	17.874	22.0	22.064	³⁵⁻³⁷

Table 4: Density ρ , isothermal compressibility β_T , volume expansivity α_p and enthalpy of vaporization Δh_v for different molecular Ethylene glycol models in comparison with experimental data^{28,40,41} at 298 K and 1 bar. The number in parentheses indicates the statistical uncertainty in the last digit.

	ρ mol/l	β_T $10^{-4}1/\text{MPa}$	α_p $10^{-4}1/\text{K}$	Δh_v kJ/mol
present model	17.339 (3)	2.44 (9)	5.3 (4)	70.90 (2)
OPLS-AA ^{38,39}	16.887	4.9	10.1	59.2
Modified OPLS-AA ¹⁷	17.226	4.2	9.5	64.3
Gubskaya and Kusalik ¹⁵	17.468	5.0	8.6	72.2
Szefczyk and Cordeiro ¹⁹	17.903	5.4	8.8	75.6
Experiment	17.888 ²⁸	3.41 ⁴⁰	6.36 ⁴¹	66.5 ²⁸

Table 5: Geometry, Lennard-Jones and point charge parameters for molecular Water models of TIP4P type, cf. Figure 7.

Model	h_1 Å	h_2 Å	α °	σ_O Å	ϵ_O/k_B K	q_O e	q_H e
TIP4P ⁵⁰	0.15000	0.9572	104.52	3.15365	78.020	-1.04000	+0.52000
TIP4P-Ew ⁵¹	0.12500	0.9572	104.52	3.16435	81.921	-1.04844	+0.52422
TIP4P/2005 ⁵²	0.15460	0.9572	104.52	3.15890	93.200	-1.11280	+0.55640
TIP4P/Ice ⁵³	0.15770	0.9572	104.52	3.16680	106.100	-1.17940	+0.58970
SPC/E ⁵⁴	0	1	109.47	3.16600	78.178	-0.84760	+0.42380
present model	0.20482	1.3338	104.52	3.11831	208.080	-0.83910	+0.41955

Table 6: Binary interaction parameter ξ , experimental saturated liquid point used for the adjustment with reference, simulation results with adjusted ξ and binary parameter k_{ij} of the Peng-Robinson EOS. The number in parentheses indicates the statistical uncertainty in the last digit.

Mixture (A + B)	ξ	T K	x_A mol/mol	p^{exp} MPa	p^{sim} MPa	y_A^{sim} mol/mol	k_{ij}
Ethylene oxide + Water	1.126	370.00	0.03	0.31 ⁶⁹	0.31 (3)	0.701 (8)	-0.1
Ethylene oxide + Ethylene glycol	1.016	378.15	0.1	0.38 ⁷²	0.38 (1)	0.999 (1)	0.01
Water + Ethylene glycol	0.800	395.15	0.466	0.084 ⁷³	0.082 (2)	0.965 (4)	-0.066

Table 7: Vapor-liquid equilibrium simulation results for binary mixtures in partial comparison to experimental vapor pressure data. The number in parentheses indicates the statistical uncertainty in the last digit.

Mixture (A + B)	T K	x_A mol/mol	p MPa	p^{exp} MPa	y_A mol/mol	ρ' mol/l	ρ'' mol/l	Δh_v kJ/mol
Ethylene oxide + Water								
	330.65	0.800	0.44 (1)	0.44 ⁶⁹	0.978 (1)	21.81 (1)	0.172 (2)	26.08 (1)
	334.35	0.300	0.48 (1)	0.44 ⁶⁹	0.974 (1)	35.98 (1)	0.189 (4)	36.46 (1)
	338.75	0.200	0.50 (2)	0.44 ⁶⁹	0.967 (1)	40.68 (1)	0.195 (6)	38.53 (1)
	350.95	0.100	0.46 (2)	0.44 ⁶⁹	0.929 (3)	46.13 (1)	0.166 (1)	40.33 (1)
	368.35	0.050	0.43 (2)	0.44 ⁶⁹	0.846 (8)	48.84 (1)	0.148 (1)	40.70 (1)
	390.85	0.020	0.38 (2)	0.44 ⁶⁹	0.61 (2)	50.15 (1)	0.123 (5)	40.42 (1)
	350.00	0.06	0.33 (2)	0.31 ⁶⁹	0.901 (6)	49.02 (1)	0.117 (7)	41.43 (1)
	350.00	0.180	0.56 (2)	–	0.944 (3)	41.37 (2)	0.218 (2)	38.66 (2)
	350.00	0.280	0.67 (2)	–	0.960 (1)	36.23 (1)	0.256 (7)	35.92 (1)
	350.00	0.500	0.71 (1)	–	0.964 (1)	28.12 (1)	0.274 (4)	30.94 (1)
	350.00	0.750	0.72 (1)	–	0.967 (1)	22.03 (1)	0.277 (3)	25.78 (1)
	350.00	0.900	0.75 (1)	–	0.977 (1)	19.37 (1)	0.288 (3)	23.07 (1)
	370.00	0.030	0.32 (1)	0.31 ⁶⁹	0.77 (1)	50.36 (1)	0.106 (4)	41.21 (1)
	370.00	0.048	0.43 (2)	0.44 ⁶⁹	0.836 (8)	49.04 (1)	0.148 (8)	40.70 (1)
	370.00	0.150	0.89 (3)	–	0.924 (2)	42.05 (1)	0.33 (1)	37.78 (1)
	370.00	0.280	1.06 (2)	–	0.940 (1)	35.31 (7)	0.394 (6)	34.48 (1)
	370.00	0.500	1.09 (1)	–	0.947 (1)	27.24 (1)	0.409 (5)	29.54 (1)
	370.00	0.720	1.10 (1)	–	0.951 (1)	21.82 (1)	0.415 (4)	24.96 (1)
	370.00	0.800	1.15 (1)	–	0.957 (1)	20.27 (1)	0.446 (3)	23.40 (1)
	370.00	0.950	1.22 (1)	–	0.980 (1)	17.82 (1)	0.467 (3)	20.94 (1)

Table 7: continued.

Mixture (A + B)	T K	x_A mol/mol	p MPa	p^{exp} MPa	y_A mol/mol	ρ' mol/l	ρ'' mol/l	Δh_v kJ/mol
Ethylene oxide + Ethylene glycol								
	360.15	0.075	0.17 (1)	0.22 ⁷²	1.0	17.04 (1)	0.059 (2)	63.47 (2)
	360.15	0.130	0.29 (1)	0.34 ⁷²	1.0	17.17 (1)	0.101 (3)	60.83 (2)
	360.15	0.200	0.53 (1)	–	1.0	17.40 (1)	0.189 (4)	58.00 (2)
	360.15	0.250	0.67 (1)	–	1.0	17.51 (1)	0.244 (4)	55.45 (2)
	360.15	0.300	0.71 (2)	–	1.0	17.59 (1)	0.259 (6)	52.72 (2)
	360.15	0.800	0.99 (1)	–	1.0	17.93 (1)	0.383 (3)	28.97 (1)
	378.15	0.051	0.20 (1)	0.21 ⁷²	1.0	16.83 (1)	0.066 (2)	63.92 (2)
	378.15	0.100	0.38 (1)	0.38 ⁷²	1.0	16.91 (1)	0.124 (5)	61.31 (2)
	378.15	0.200	0.92 (2)	–	1.0	17.22 (1)	0.323 (7)	56.61 (2)
	378.15	0.250	1.13 (2)	–	1.0	17.33 (1)	0.409 (7)	54.07 (2)
	378.15	0.300	1.22 (3)	–	1.0	17.41 (1)	0.45 (1)	51.21 (2)
	378.15	0.800	1.47 (1)	–	1.0	17.40 (1)	0.647 (4)	24.07 (4)
Water + Ethylene glycol								
	383.15	0.200	0.011 (1)	0.029 ⁷³	0.881 (9)	19.53 (1)	0.0033 (1)	63.61 (2)
	383.15	0.401	0.032 (1)	–	0.97 (1)	23.41 (1)	0.0102 (2)	59.94 (3)
	383.15	0.500	0.047 (1)	–	0.987 (2)	25.89 (1)	0.0149 (2)	57.53 (2)
	383.15	0.600	0.063 (1)	–	1.0	28.87 (1)	0.0199 (3)	54.84 (2)
	383.15	0.800	0.094 (1)	–	1.0	37.25 (1)	0.0302 (4)	48.19 (1)
	395.15	0.200	0.019 (1)	–	0.873 (9)	19.38 (1)	0.0059 (1)	62.81 (2)
	395.15	0.401	0.049 (1)	–	0.967 (2)	23.21 (1)	0.0151 (2)	59.05 (2)
	395.15	0.466	0.064 (2)	0.084 ⁷³	0.97 (2)	24.81 (1)	0.0198 (6)	57.43 (3)
	395.15	0.600	0.098 (1)	–	0.990 (1)	28.61 (1)	0.0304 (3)	53.89 (2)
	395.15	0.800	0.137 (1)	–	1.0	36.81 (1)	0.0427 (1)	47.37 (1)

Table 8: Henry’s law constant of Ethylene oxide in mixtures of Ethylene glycol + Water from molecular simulation. x'_{EG} are the gas free liquid mole fractions. The number in parentheses indicates the statistical uncertainty in the last digits.

x'_{EG} / mol/mol	H_{EO} / MPa			
	$T=350$ K	$T=400$ K	$T=450$ K	$T=500$ K
0.0	6.9 (3.0)	14.9 (2.2)	23.7 (1.4)	32.1 (1.0)
0.041	4.8 (5.0)			27.0 (1.0)
0.07	4.5 (5.0)			25.0 (1.0)
0.1	3.6 (5.0)			24.0 (1.0)
0.136	4.2 (5.0)			23.0 (1.0)

List of Figures

1	Geometry of the present Ethylene glycol model, where all sites are situated in a plane. Lennard-Jones sites are indicated by ●, point charges by ○.	38
2	Saturated densities; present simulation data: ● Ethylene oxide, ▲ Ethylene glycol, ■ Water; — correlations of experimental data. ²⁸	39
3	Vapor pressure; present simulation data: ● Ethylene oxide, ▲ Ethylene glycol, ■ Water; — correlations of experimental data. ²⁸	40
4	Enthalpy of vaporization; present simulation data: ● Ethylene oxide, ▲ Ethylene glycol, ■ Water; — correlations of experimental data. ²⁸ The points at the bottom indicate the critical temperature of the present models.	41
5	Relative deviations of vapor-liquid equilibrium properties from correlations of experimental data ²⁸ ($\delta z = (z_i - z_{cor})/z_{cor}$) for Ethylene glycol: ● present simulation data; □ simulation data by Ferrando et al.; ²⁰ + experimental data. ³¹⁻³⁴ Top: saturated liquid density, center: vapor pressure, bottom: enthalpy of vaporization. . . .	42
6	Site-site pair correlation functions of Ethylene glycol at 298 K and 1 bar: — $g_{OO}(r)$, - - $g_{CO}(r)$, ··· $g_{CC}(r)$	43
7	Geometry of TIP4P type Water models, where all sites are situated in a plane. Lennard-Jones sites are indicated by ●, point charges by ○.	44
8	Relative deviations of vapor-liquid equilibrium properties from correlations of experimental data ²⁸ ($\delta z = (z_i - z_{cor})/z_{cor}$) for Water: ● present model simulation data; ○ TIP4P simulation data by Lísal et al.; ⁵⁶ □ SPC/E simulation data by Guisani and Guillot; ⁵⁷ ▲ TIP4P/2005 simulation data by Vega et al.; ⁵⁸ △ TIP4P-Ew simulation data by Baranyai et al.; ⁵⁹ + experimental data. ³⁵⁻³⁷ Top: saturated liquid density, center: vapor pressure, bottom: enthalpy of vaporization. Note that simulation data for the enthalpy of vaporization are only available at 298 K for the TIP4P/2005 and the SPC/E model. ⁴⁷	45
9	Oxygen-oxygen pair correlation function of water at 298 K and 1 bar: — $g_{OO}(r)$	46

10	Second virial coefficient; Ethylene Oxide: ● present model; ○ experimental data; ⁶¹ - - DIPPR correlation; ²⁸ Ethylene glycol: ▲ present model; △ prediction by Abusleme and Vera; ⁶³ - · - DIPPR correlation; ²⁸ Water: ■ present model; — equation of state by Wagner and Pruss. ⁶²	47
11	Isobaric vapor-liquid phase diagram of Ethylene oxide + Water at 0.4428 MPa: + experimental data; ⁶⁹ ● present simulation data with $\xi = 1.126$; — Peng-Robinson EOS with $k_{ij} = -0.1$	48
12	Isothermal vapor-liquid phase diagram of Ethylene oxide + Water at 350 and 370 K: + experimental data; ⁶⁹ ■, ● present simulation data with $\xi = 1.126$; — Peng- Robinson EOS with $k_{ij} = -0.1$	49
13	Henry's law constant of Ethylene oxide in Water: ● present simulation data with $\xi = 1.126$. The straight line is a guide for the eye. The enthalpy of absorption of Ethylene oxide in Water in the absence of chemical reactions was found to be -15 (±5) kJ/mol from this data. The number in parentheses is the uncertainty of the enthalpy of absorption.	50
14	Isothermal vapor-liquid phase diagram of Ethylene oxide + Ethylene glycol at 360.15 and 378.15 K: + experimental data; ⁷² ■, ● present simulation data with ξ = 1.016; — Peng-Robinson EOS with $k_{ij} = 0.01$	51
15	Isothermal vapor-liquid phase diagram of Water + Ethylene glycol at 383.15 and 395.15 K: + experimental data; ⁷³ ■, ● present simulation data with $\xi = 0.8$; — Peng-Robinson EOS with $k_{ij} = -0.066$	52
16	Henry's law constant of Ethylene oxide in liquid mixtures of Water + Ethylene glycol as a function of the mole fraction x'_{EG} of Ethylene glycol (on a ethylene oxide-free basis) at 350 and 500 K: ■, ● present simulation data. The lines are guides for the eye.	53

Figure 1: Geometry of the present Ethylene glycol model, where all sites are situated in a plane. Lennard-Jones sites are indicated by ●, point charges by ○.

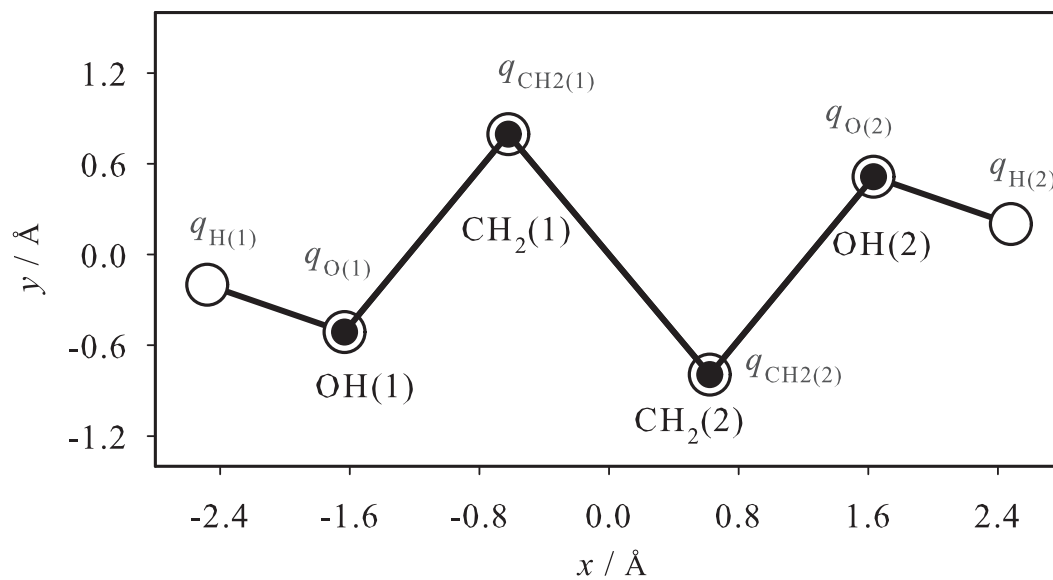


Figure 2: Saturated densities; present simulation data: ● Ethylene oxide, ▲ Ethylene glycol, ■ Water; — correlations of experimental data.²⁸

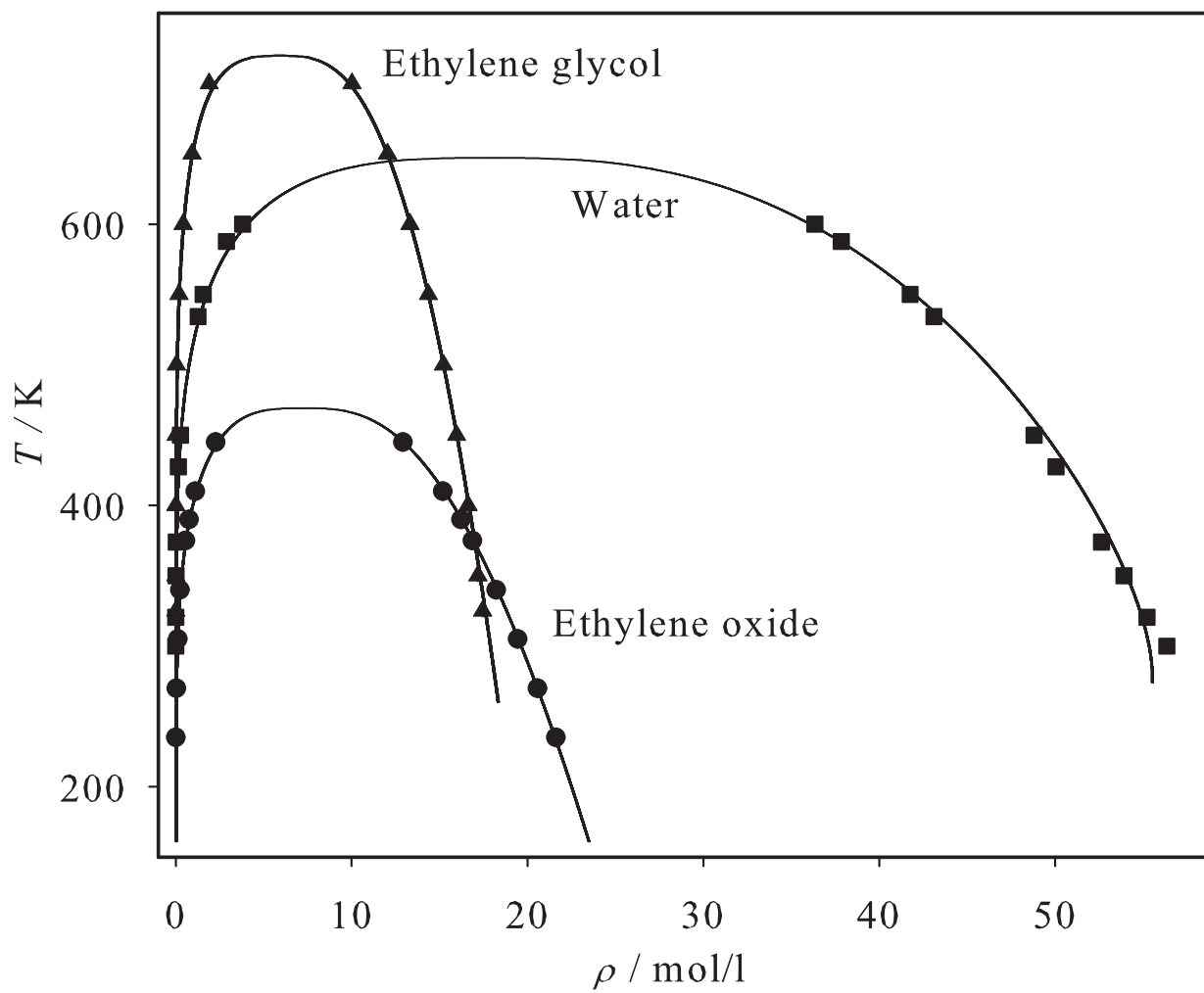


Figure 3: Vapor pressure; present simulation data: ● Ethylene oxide, ▲ Ethylene glycol, ■ Water; — correlations of experimental data.²⁸

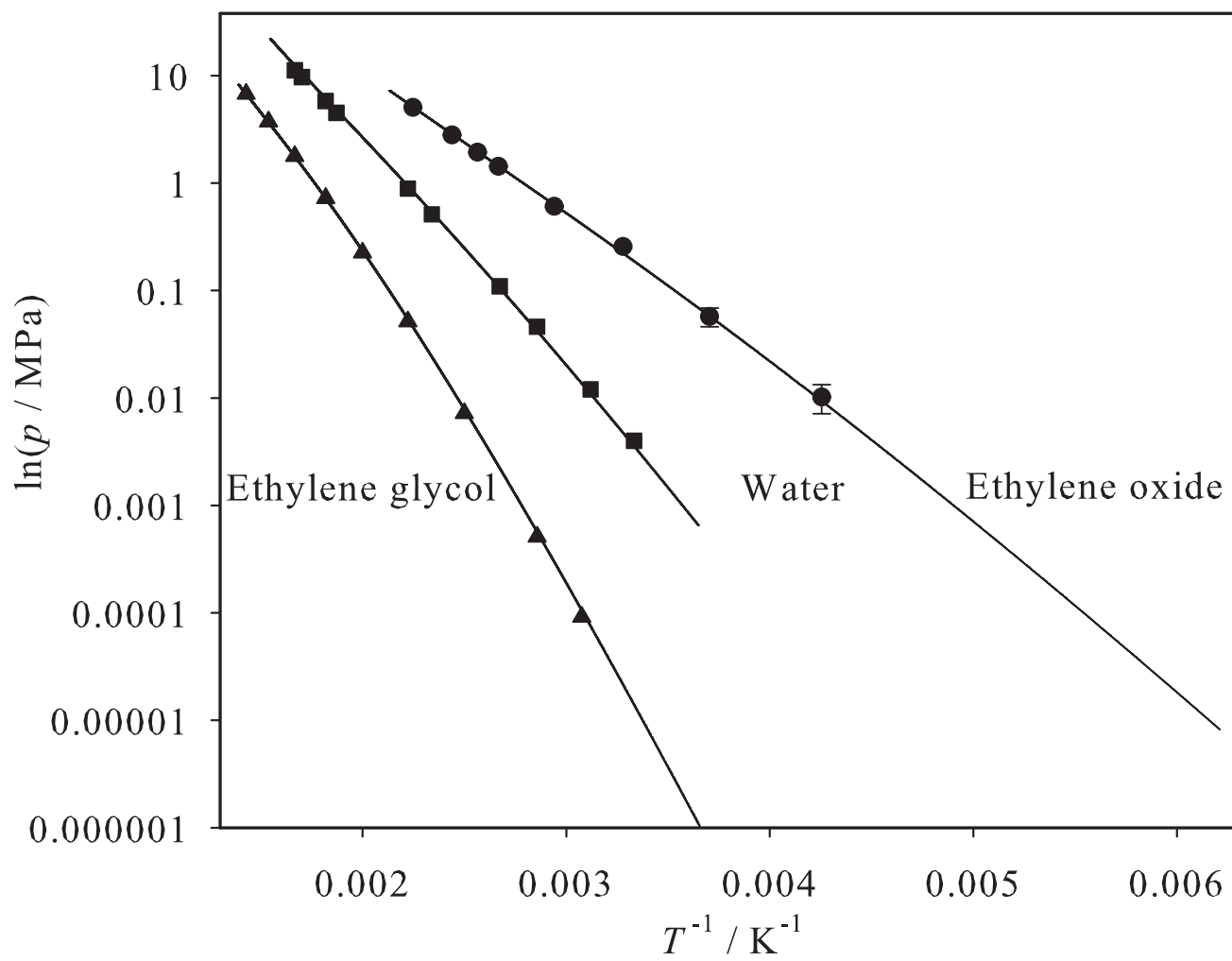


Figure 4: Enthalpy of vaporization; present simulation data: ● Ethylene oxide, ▲ Ethylene glycol, ■ Water; — correlations of experimental data.²⁸ The points at the bottom indicate the critical temperature of the present models.

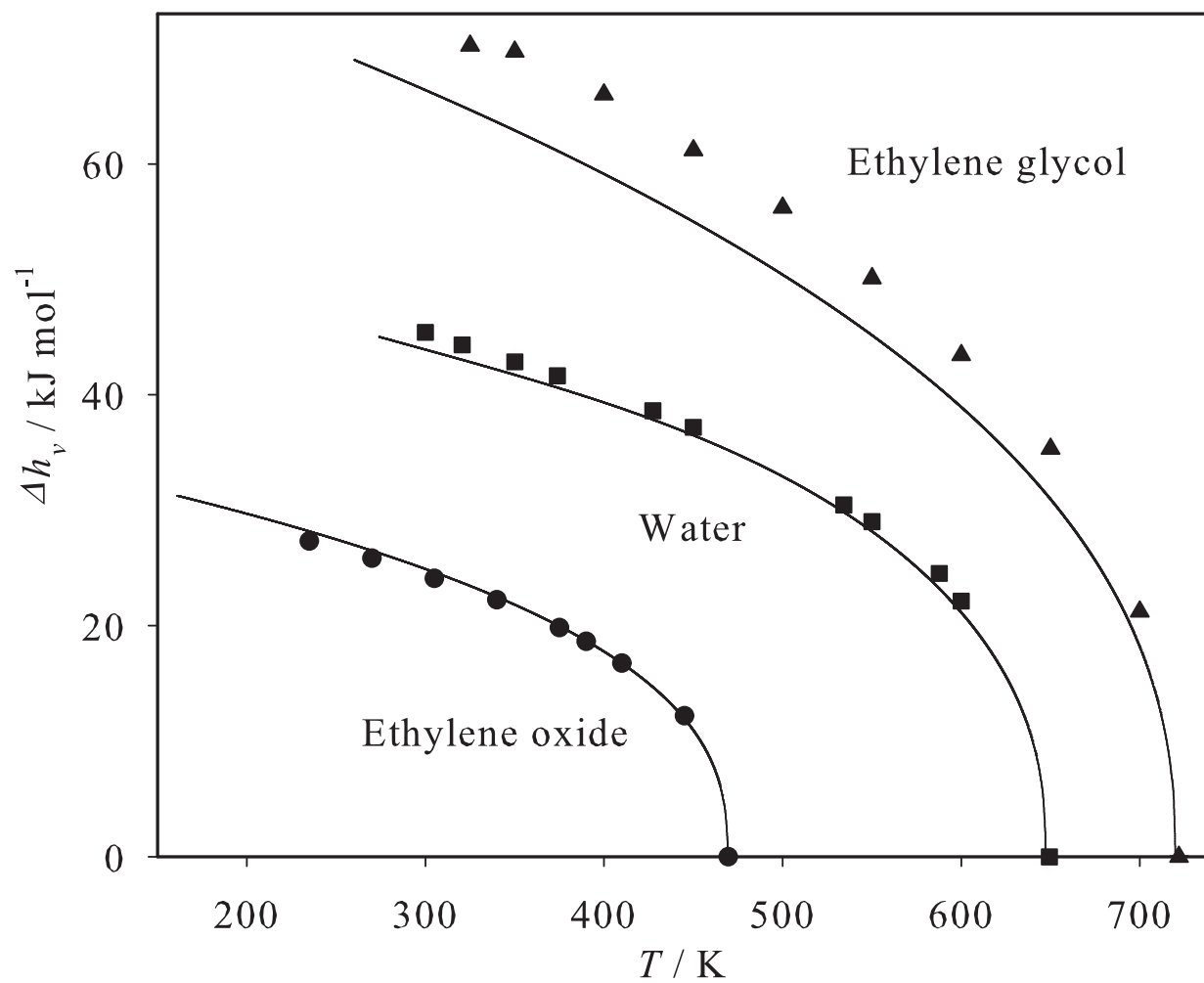


Figure 5: Relative deviations of vapor-liquid equilibrium properties from correlations of experimental data²⁸ ($\delta z = (z_i - z_{cor})/z_{cor}$) for Ethylene glycol: ● present simulation data; □ simulation data by Ferrando et al.;²⁰ + experimental data.³¹⁻³⁴ Top: saturated liquid density, center: vapor pressure, bottom: enthalpy of vaporization.

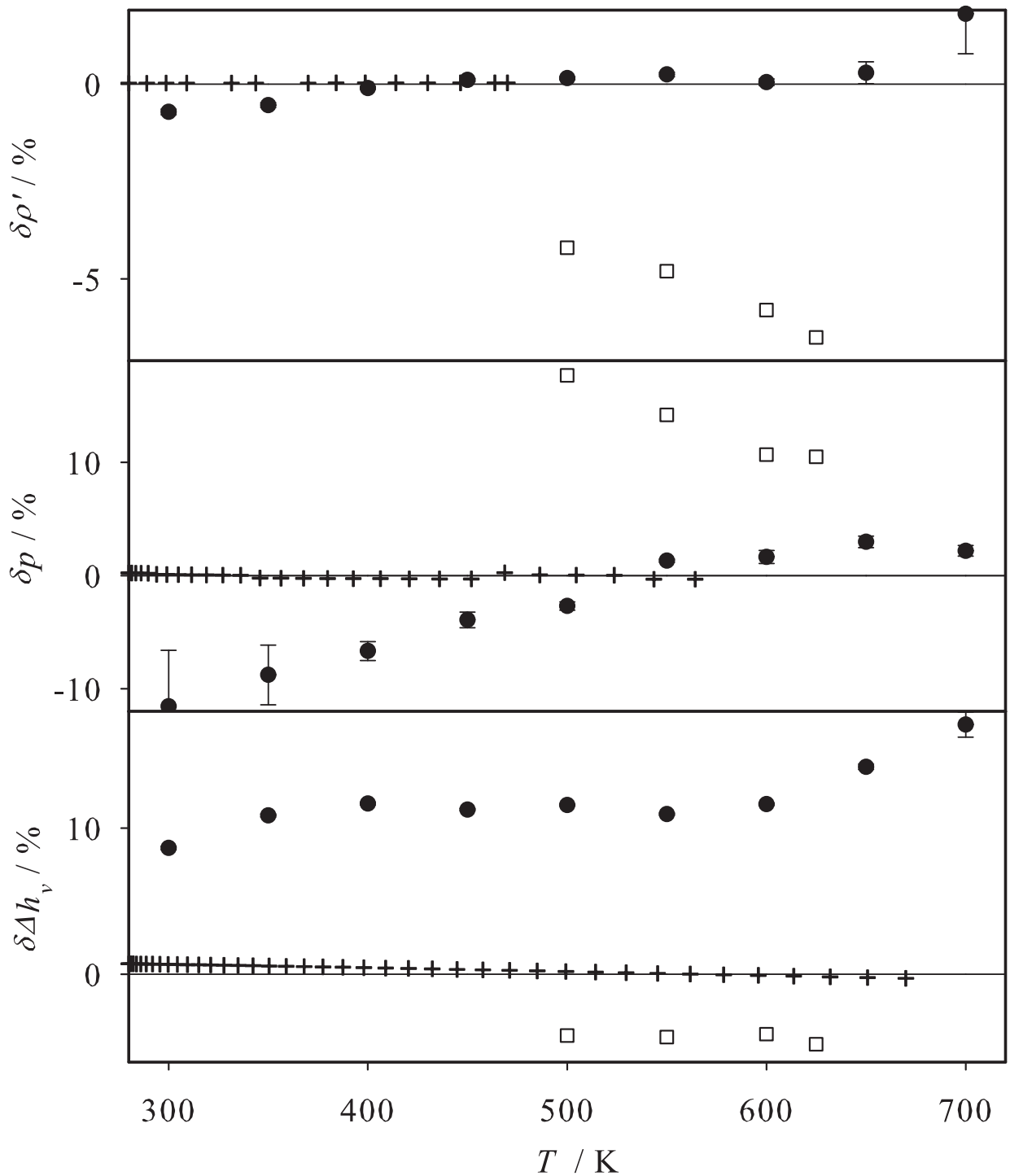


Figure 6: Site-site pair correlation functions of Ethylene glycol at 298 K and 1 bar: — $g_{OO}(r)$, - - $g_{CO}(r)$, \cdots $g_{CC}(r)$.

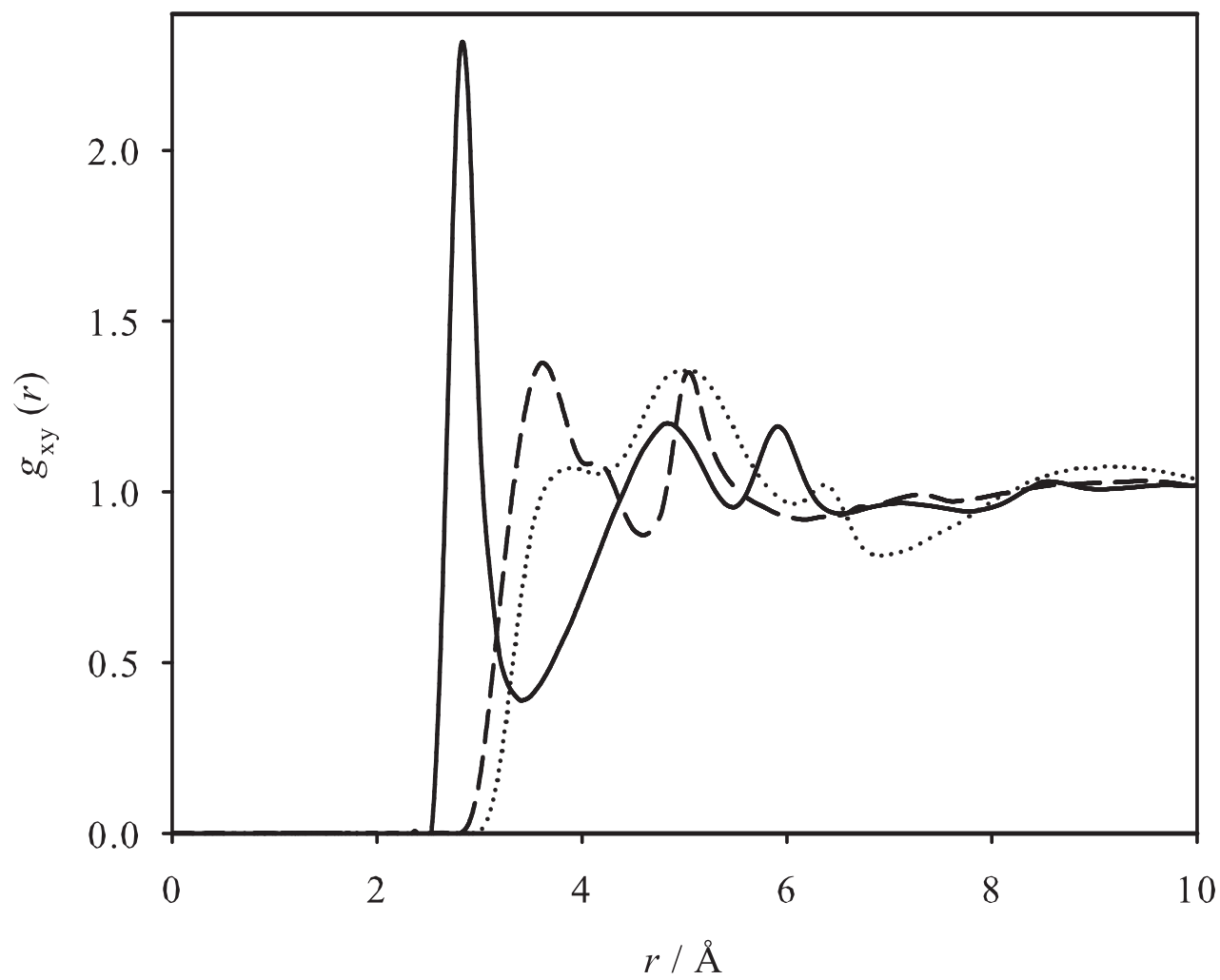


Figure 7: Geometry of TIP4P type Water models, where all sites are situated in a plane. Lennard-Jones sites are indicated by \bullet , point charges by \circ .

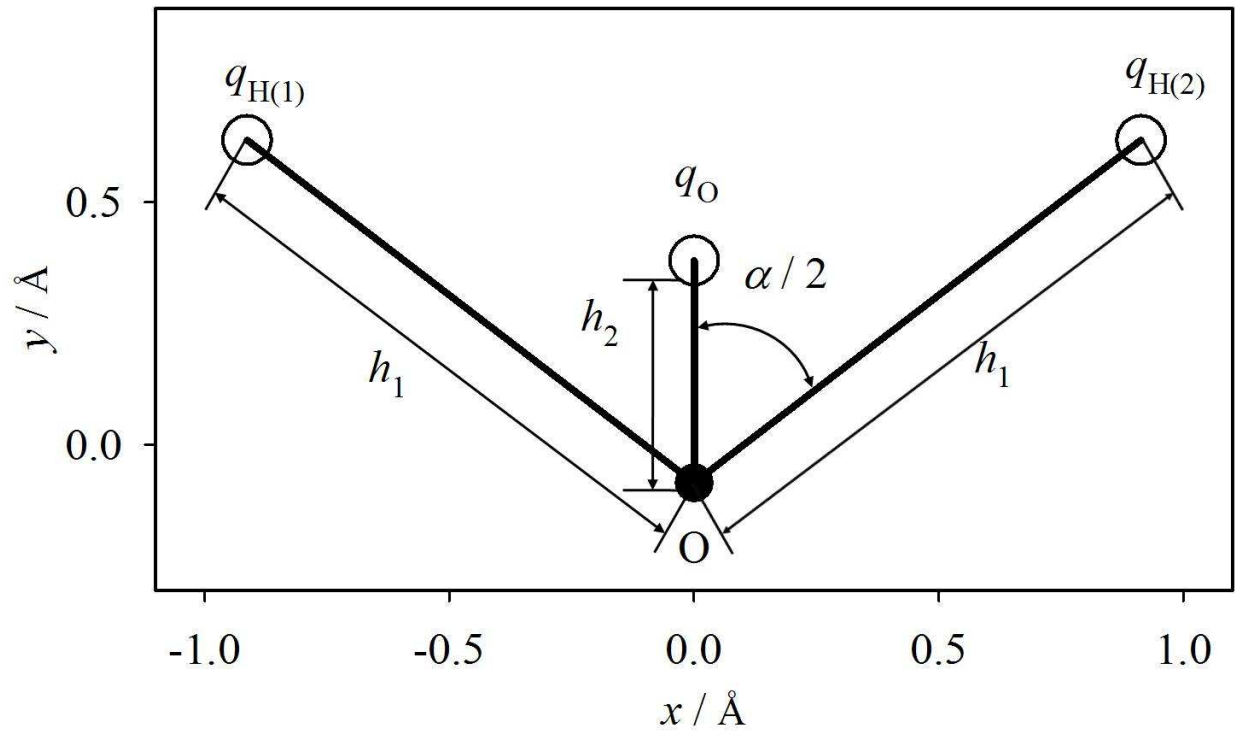


Figure 8: Relative deviations of vapor-liquid equilibrium properties from correlations of experimental data²⁸ ($\delta z = (z_i - z_{\text{cor}})/z_{\text{cor}}$) for Water: ● present model simulation data; ○ TIP4P simulation data by Lísal et al.;⁵⁶ □ SPC/E simulation data by Guissani and Guillot;⁵⁷ ▲ TIP4P/2005 simulation data by Vega et al.;⁵⁸ △ TIP4P-Ew simulation data by Baranyai et al.;⁵⁹ + experimental data.^{35–37} Top: saturated liquid density, center: vapor pressure, bottom: enthalpy of vaporization. Note that simulation data for the enthalpy of vaporization are only available at 298 K for the TIP4P/2005 and the SPC/E model.⁴⁷

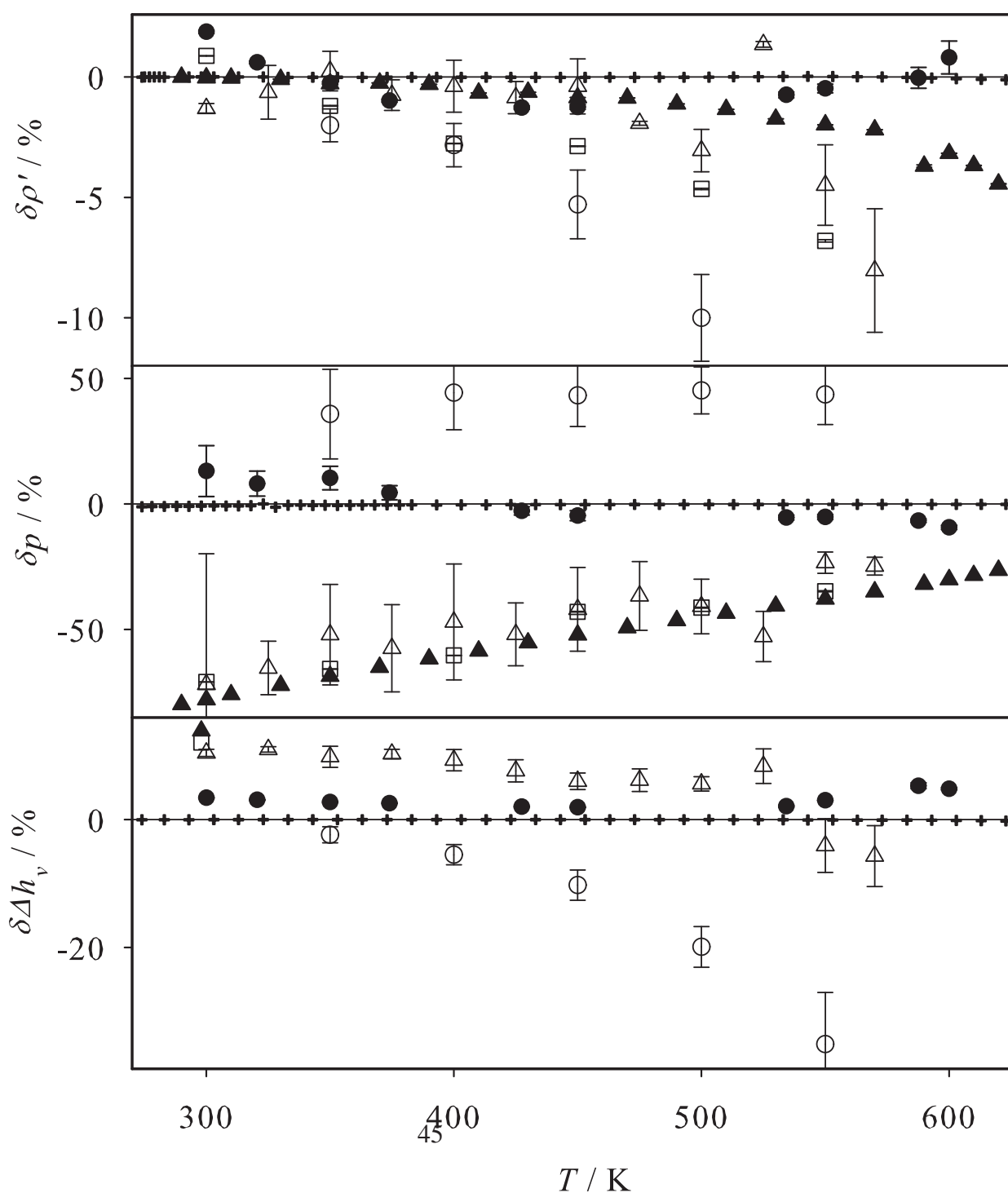


Figure 9: Oxygen-oxygen pair correlation function of water at 298 K and 1 bar: — $g_{OO}(r)$.

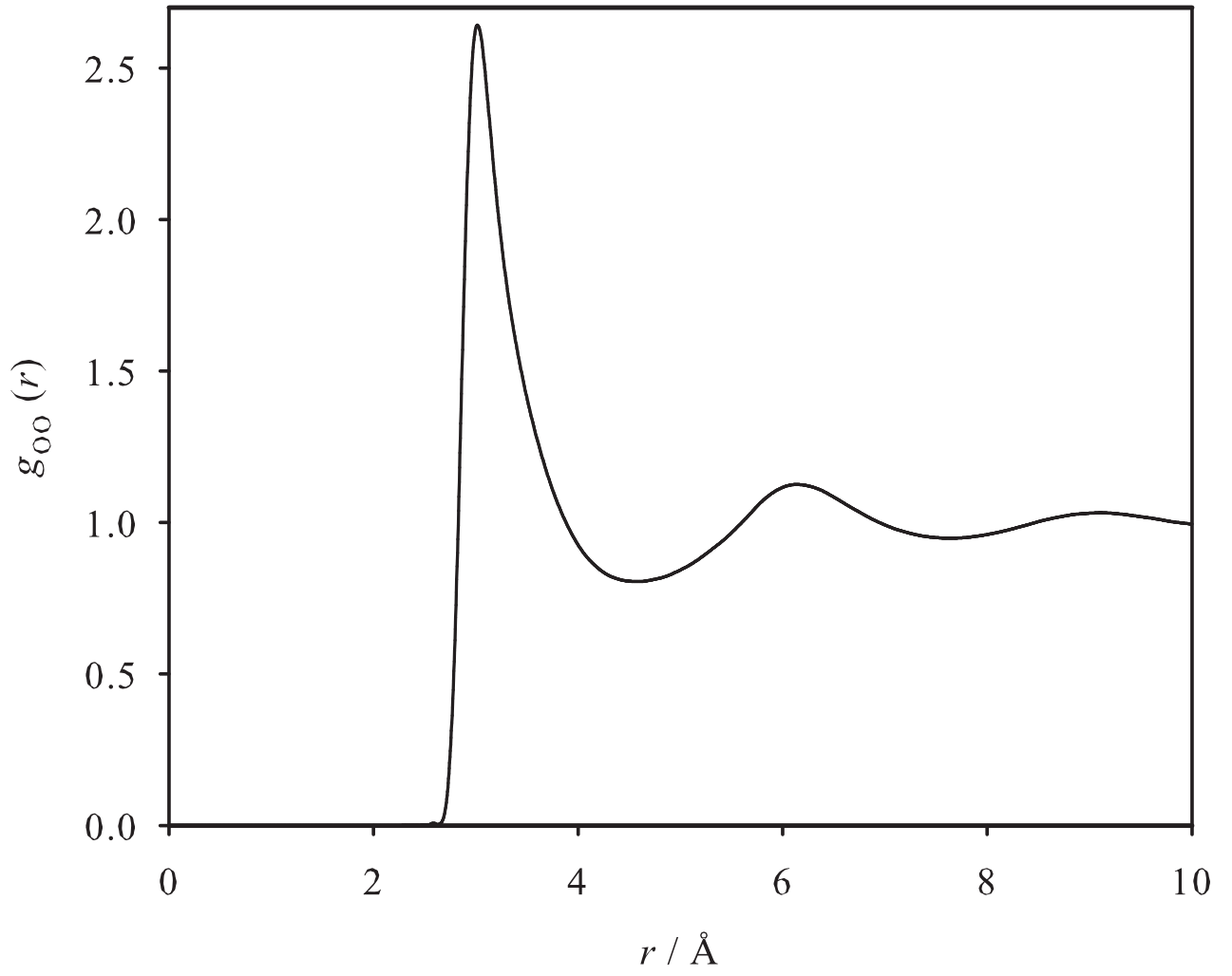


Figure 10: Second virial coefficient; Ethylene Oxide: ● present model; ○ experimental data;⁶¹ - - DIPPR correlation;²⁸ Ethylene glycol: ▲ present model; △ prediction by Abusleme and Vera;⁶³ - · - DIPPR correlation;²⁸ Water: ■ present model; — equation of state by Wagner and Pruss.⁶²

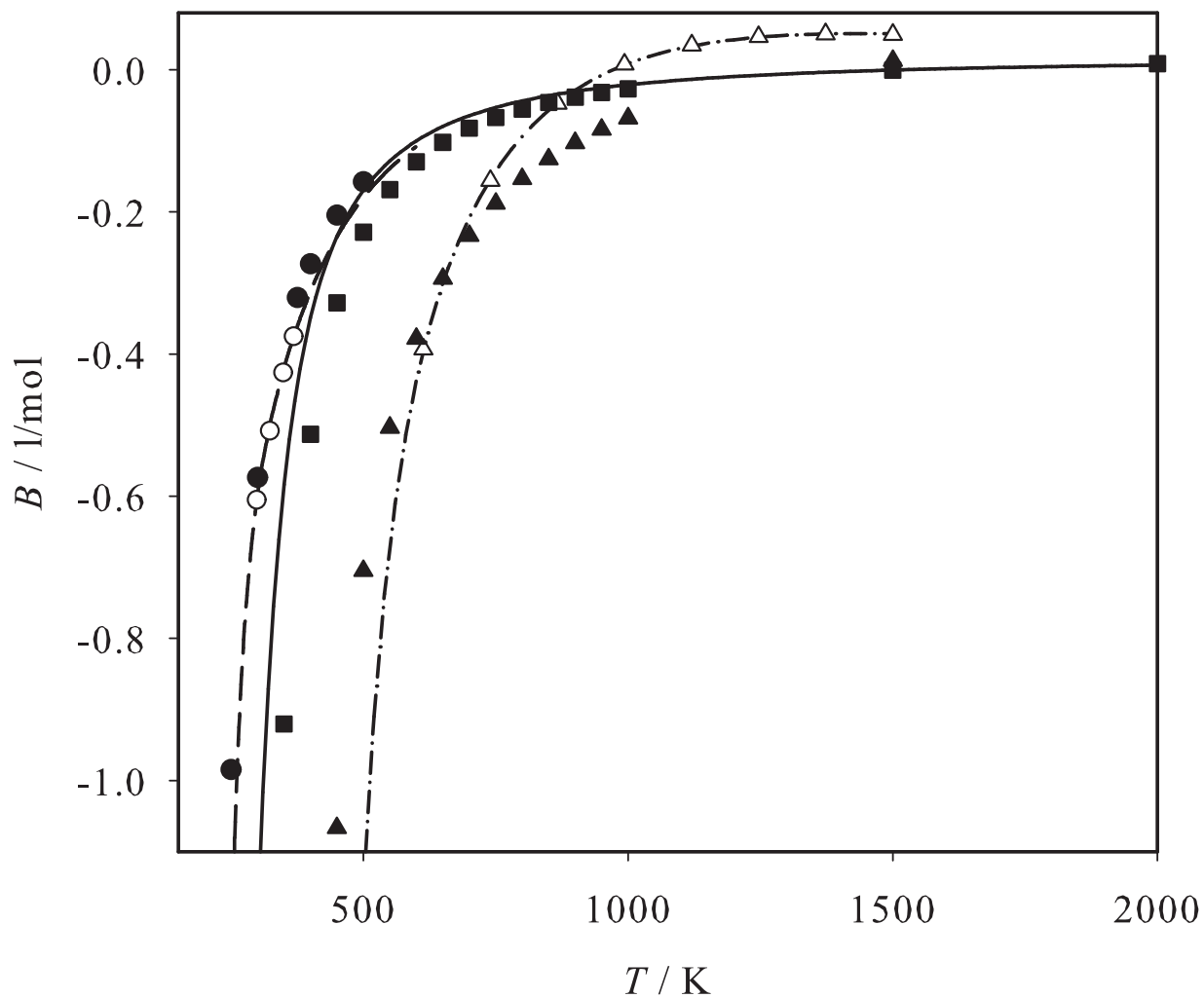


Figure 11: Isobaric vapor-liquid phase diagram of Ethylene oxide + Water at 0.4428 MPa: + experimental data;⁶⁹ ● present simulation data with $\xi = 1.126$; — Peng-Robinson EOS with $k_{ij} = -0.1$.

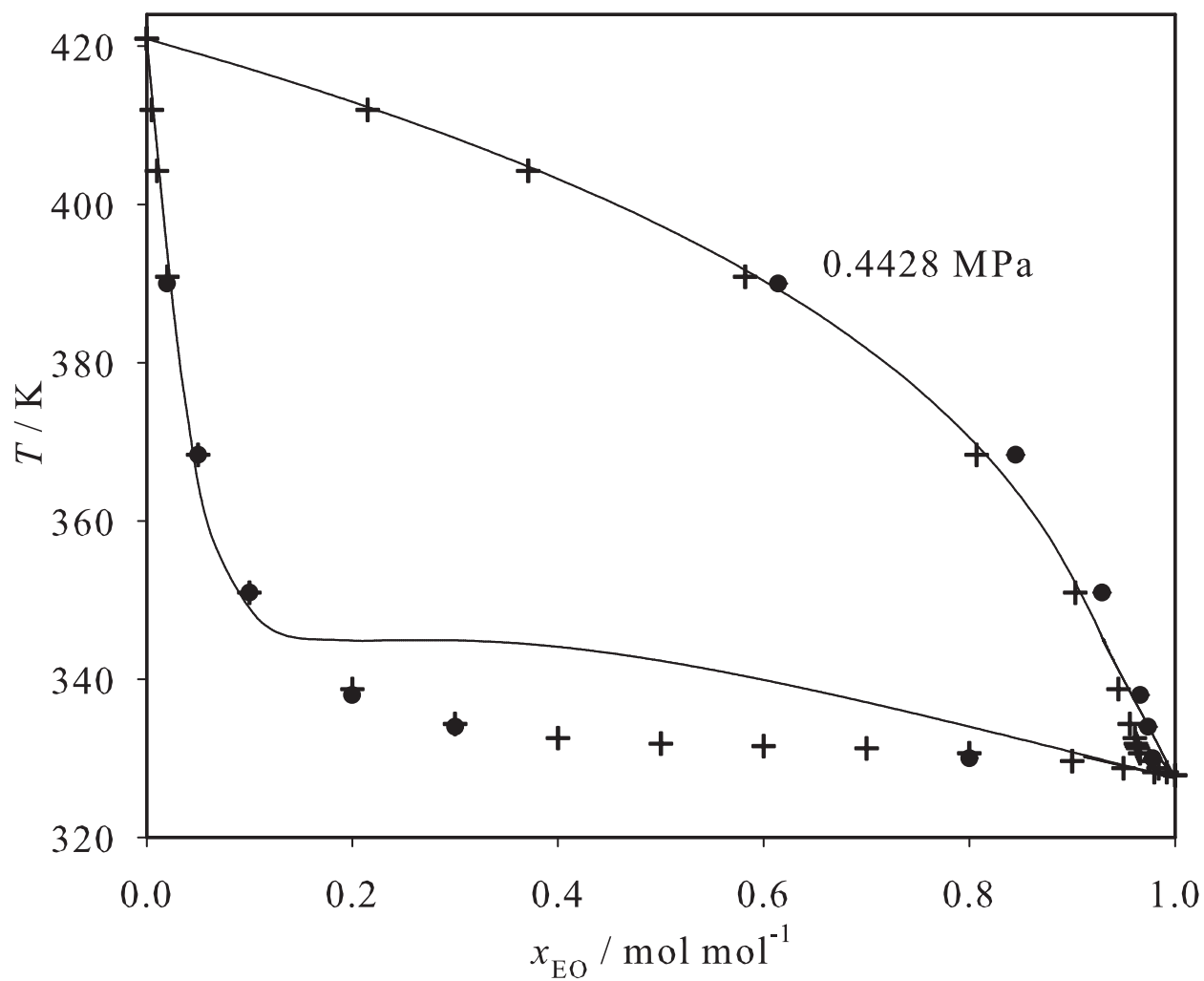


Figure 12: Isothermal vapor-liquid phase diagram of Ethylene oxide + Water at 350 and 370 K: + experimental data;⁶⁹ ■, ● present simulation data with $\xi = 1.126$; — Peng-Robinson EOS with $k_{ij} = -0.1$.

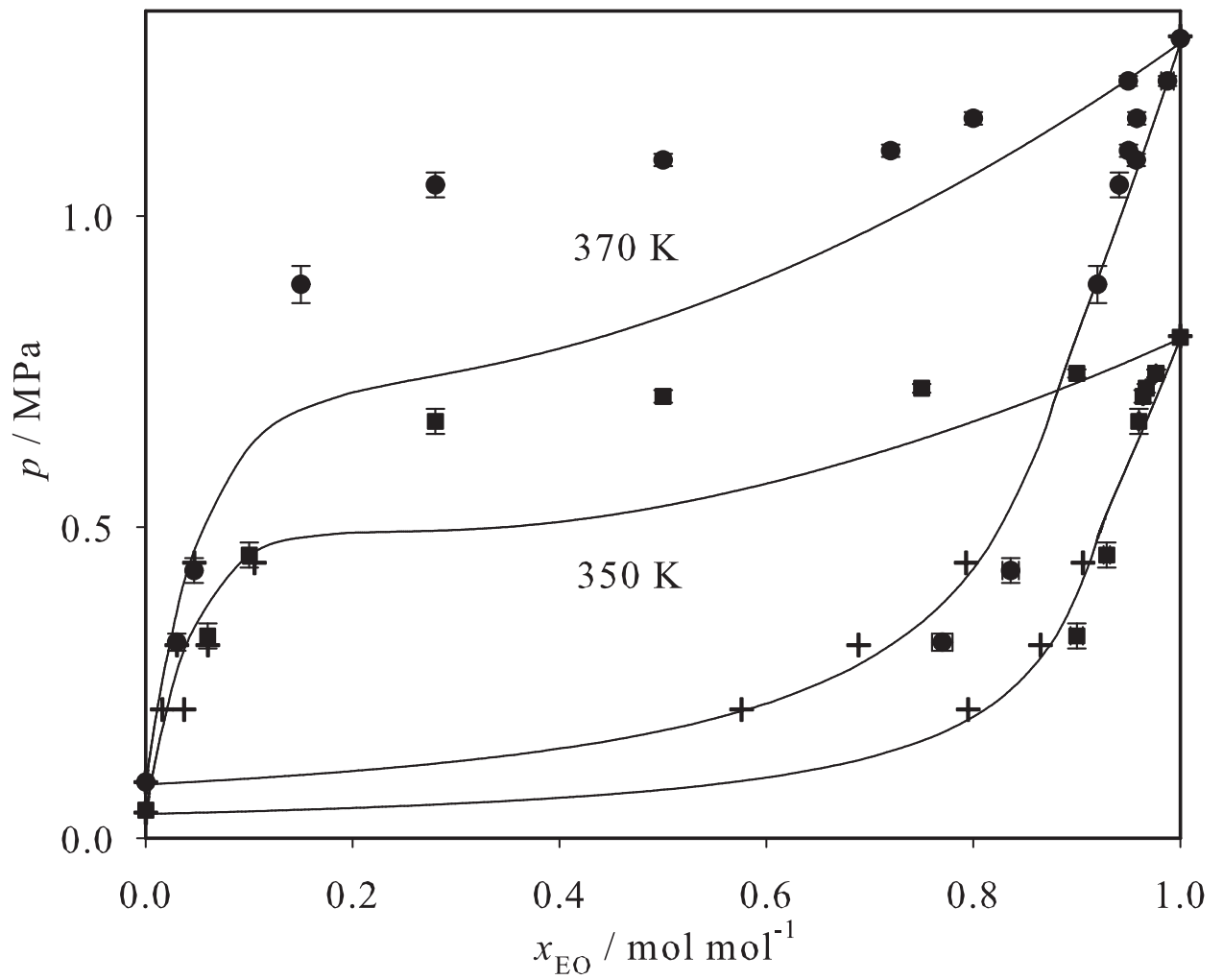


Figure 13: Henry's law constant of Ethylene oxide in Water: ● present simulation data with $\xi = 1.126$. The straight line is a guide for the eye. The enthalpy of absorption of Ethylene oxide in Water in the absence of chemical reactions was found to be $-15 (\pm 5)$ kJ/mol from this data. The number in parentheses is the uncertainty of the enthalpy of absorption.

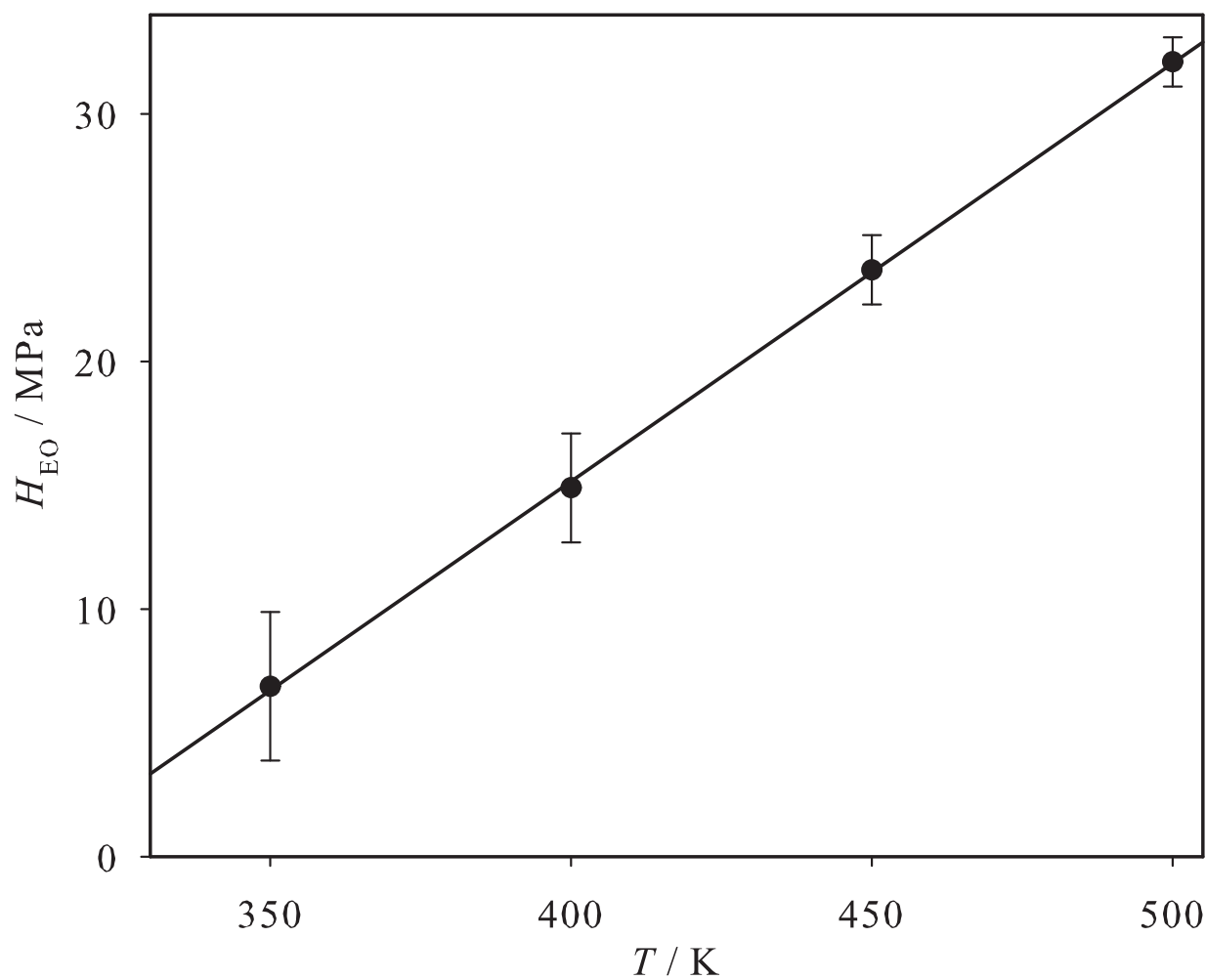


Figure 14: Isothermal vapor-liquid phase diagram of Ethylene oxide + Ethylene glycol at 360.15 and 378.15 K: + experimental data;⁷² ■, ● present simulation data with $\xi = 1.016$; — Peng-Robinson EOS with $k_{ij} = 0.01$.

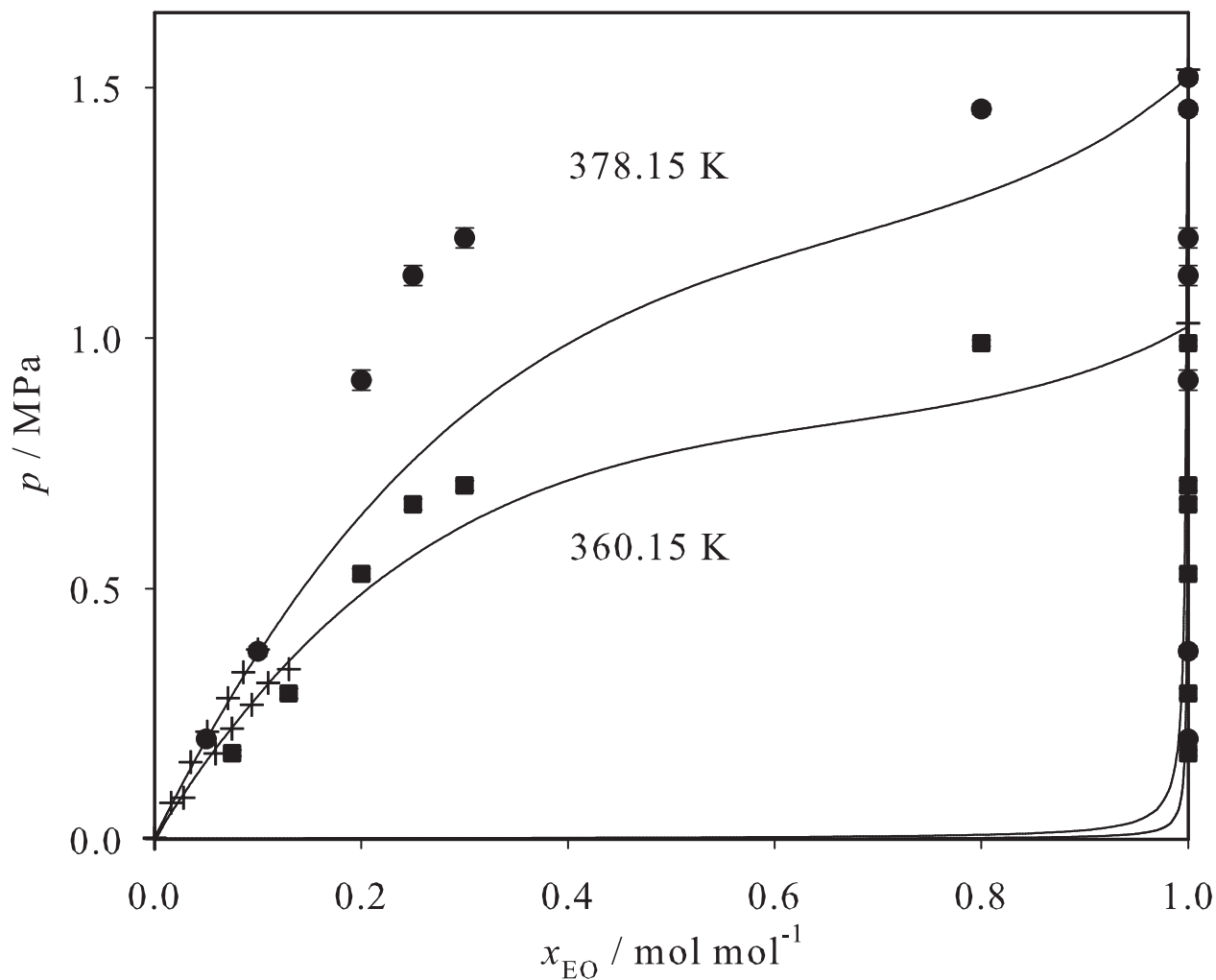


Figure 15: Isothermal vapor-liquid phase diagram of Water + Ethylene glycol at 383.15 and 395.15 K: + experimental data;⁷³ ■, ● present simulation data with $\xi = 0.8$; — Peng-Robinson EOS with $k_{ij} = -0.066$.

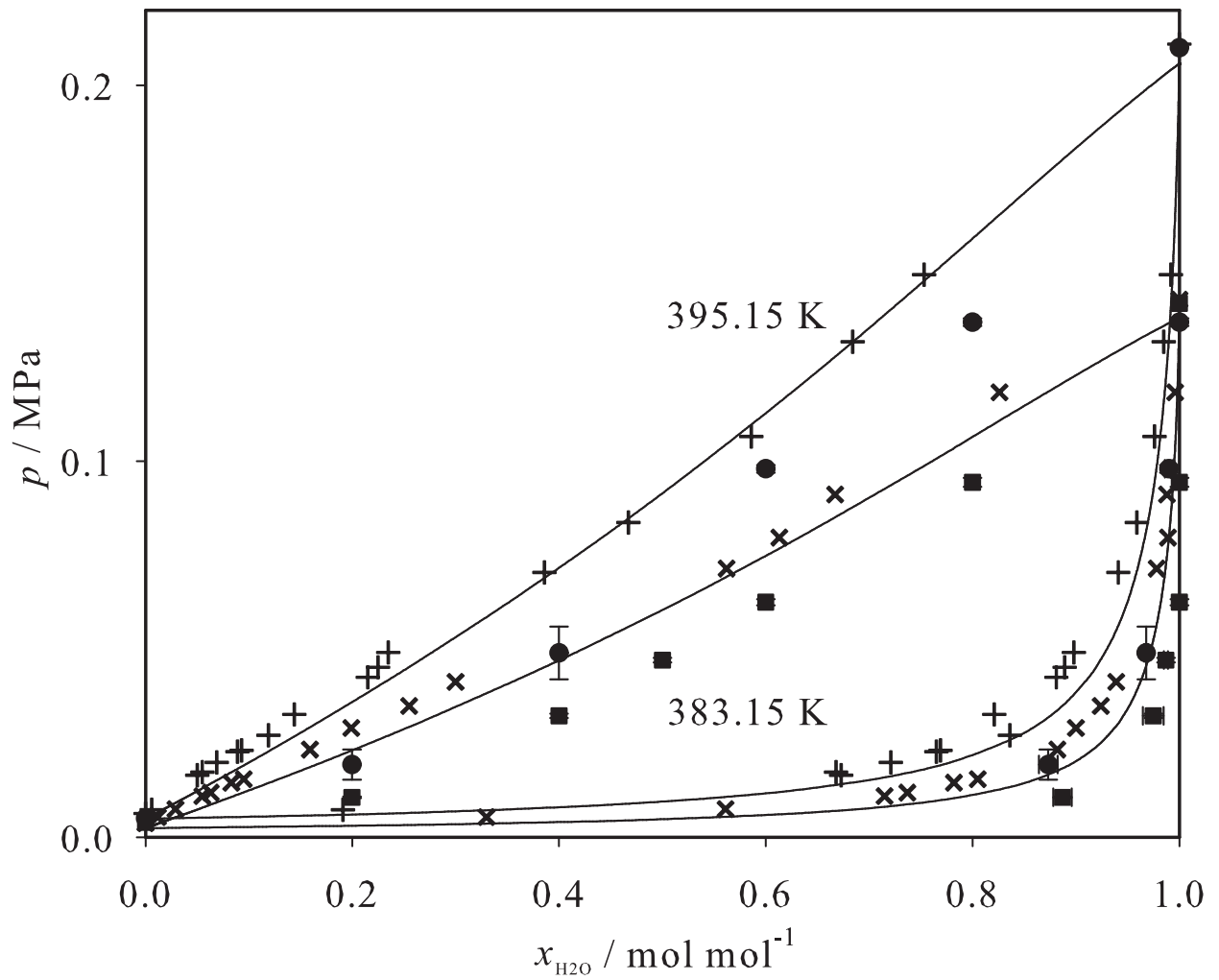


Figure 16: Henry's law constant of Ethylene oxide in liquid mixtures of Water + Ethylene glycol as a function of the mole fraction x'_{EG} of Ethylene glycol (on a ethylene oxide-free basis) at 350 and 500 K: ■, ● present simulation data. The lines are guides for the eye.

